Soft lubrication: The elastohydrodynamics of nonconforming and conforming contacts

J. M. Skotheim and L. Mahadevan
Department of Applied Mathematics and Theoretical Physics, Centre for Mathematical Sciences, Cambridge CB3 0WA, United Kingdom and Division of Engineering and Applied Sciences, Harvard University, Pierce Hall, 29 Oxford Street, Cambridge, Massachusetts 02138

(Received 13 December 2004; accepted 13 May 2005; published online 2 September 2005)

We study the lubrication of fluid-immersed soft interfaces and show that elastic deformation couples tangential and normal forces and thus generates lift. We consider materials that deform easily, due to either geometry (e.g., a shell) or constitutive properties (e.g., a gel or a rubber), so that the effects of pressure and temperature on the fluid properties may be neglected. Four different system geometries are considered: a rigid cylinder moving parallel to a soft layer coating a rigid substrate; a soft cylinder moving parallel to a rigid substrate; a cylindrical shell moving parallel to a rigid substrate; and finally a cylindrical conforming journal bearing coated with a thin soft layer. In addition, for the particular case of a soft layer coating a rigid substrate, we consider both elastic and poroelastic material responses. For all these cases, we find the same generic behavior: there is an optimal combination of geometric and material parameters that maximizes the dimensionless normal force as a function of the softness parameter η=hydrodynamic pressure/elastic stiffness =surface deflection/gap thickness, which characterizes the fluid-induced deformation of the interface. The corresponding cases for a spherical slider are treated using scaling concepts. © *2005 American Institute of Physics*. [DOI: 10.1063/1.1985467]

I. INTRODUCTION

The reduction of friction in practical applications has been studied since antiquity. Pictographs found in Uruk, located in modern day Iraq, have been dated to ca. 3000 B.C. and illustrate the transition from sleds to wheels.[1] While this advance certainly reduced friction, further reductions were possible upon the introduction of a viscous lubricating fluid in the axle joints. The theoretical underpinnings of fluid lubrication in such geometries can be traced back to the work of Reynolds,[2] who studied the mechanics of fluid flow through a thin gap using an approximation to the Stokes' equations, now known as lubrication theory. Recent efforts in this technologically important problem have focused on modifications of Reynolds' lubrication theory to account for elastohydrodynamic effects (elastic surface deformation due to fluid pressure), piezoviscous behavior (lubricant viscosity change due to high pressure), and thermoviscous behavior (lubricant viscosity change due to frictional heating).[1,3–6]

Inspired by a host of applications in physical chemistry, polymer physics, and biolubrication, in this paper we focus on the elastohydrodynamics of soft interfaces, which deform easily thereby precluding piezoviscous and thermoviscous effects. There have been a number of works in these areas in the context of specific problems such as cartilage biomechanics,[7–9] the motion of red blood cells in capillaries,[10–18] the elastohydrodynamics of rubber-like elastomers,[19,20] polymer brushes,[21,22] and vesicles.[23,24] Another related phenomenon is that of a bubble rising slowly near a wall; the fluid pressure deforms the bubble's surface, which leads to a hydrodynamic force repelling the bubble from the wall.[25,26] Instead of focusing on specific applications, here we address a slightly different set of questions: How can one generate lift between soft sliding surfaces to increase separation and reduce wear? What is the role of geometry in determining the behavior of such systems? How do material properties influence the elastohydrodynamics? Are there optimal combinations of the geometry and the material properties that maximize the lift force? Can the study of soft lubrication lead to improved engineering designs? And finally, how is soft lubrication relevant to the study of real biological systems?

To address some of these questions, we start with the simple case of two fluid-lubricated rigid nonconforming surfaces sliding past one another at a velocity V as shown in Fig. 1. The force on the slider is dominated by viscous stresses and pressure in the narrow contact zone. For a Newtonian fluid, the Stokes equations (valid in the gap) are reversible in time t, so that the transformation $t \to -t$ implies the transformations of the velocity $V \to -V$ and the normal force $L \to -L$. In the vicinity of the contact region nonconforming surfaces are symmetric which implies that these flows are identical and therefore $L=0$. Elastohydrodynamics alters this picture qualitatively. In front of the slider the pressure is positive and pushes down the substrate, while behind the slider the pressure is negative and pulls up the substrate. As the solid deforms, the symmetry of the gap profile is broken, leading to a normal force that pushes the cylinder away from the substrate.

This picture applies naturally to soft interfaces, which arise either due to the properties of the material involved, as in the case of gels, or the underlying geometry, as in the case of thin shells. In Sec. III, we study the normal-tangential coupling of a nonconforming contact coated with a thin com-

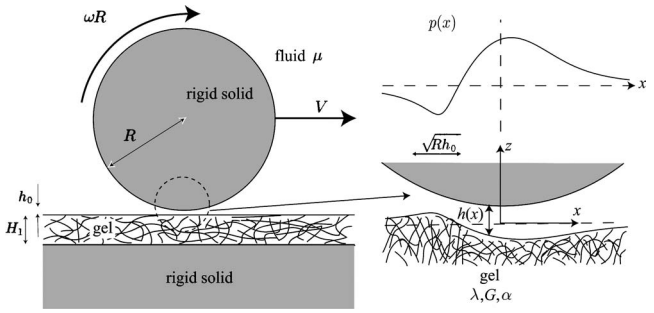

FIG. 1. A solid cylinder moves through a liquid of viscosity μ above a thin gel layer of thickness H_l that covers a rigid solid substrate. The asymmetric pressure distribution pushes down on the gel when the fluid pressure in the gap is positive while pulling up the gel when the pressure is negative. The asymmetric traction breaks the symmetry of the gap thickness profile $h(x)$ thus giving rise to a repulsive force of hydrodynamic origin. The pressure profile and the gap thickness shown here are calculated for a thin elastic layer (Sec. III) for a dimensionless deflection $\eta=10$.

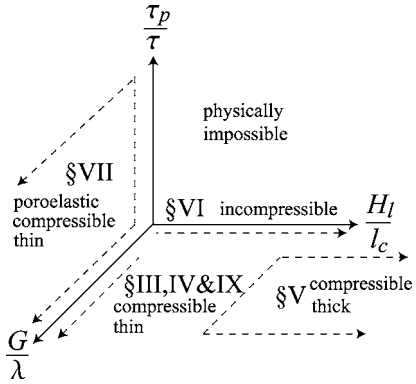

FIG. 2. Overview of the different geometries and elastic materials considered. G and λ are the Lamé coefficients of the linear elastic material, where $G/\lambda=0$ corresponds to an incompressible material, H_l is the depth of the elastic layer coating a rigid surface, l_c is the contact length, τ_p is the time scale over which stress relaxes in a poroelastic medium (a material composed of an elastic solid skeleton and an interstitial viscous fluid), and $\tau=l_c/V$ is the time scale of the motion. Section III treats normal-tangential coupling of nonconforming contacts coated with a thin compressible elastic layer. Section IV treats normal-tangential coupling of higher order degenerate contacts coated with a thin compressible elastic layer. Section V treats normal-tangential coupling of nonconforming contacts coated with a thick compressible elastic layer. Section VI treats normal-tangential coupling of nonconforming contacts coated with an incompressible elastic layer. Section VII treats normal-tangential coupling of nonconforming contacts coated with a thin compressible poroelastic layer. Section VIII treats normal-tangential coupling of nonconforming contacts between a rigid solid and a cylindrical shell. Section IX treats elastohydrodynamic effects due to coating a journal bearing with a thin compressible elastic layer. Section X treats elastohydrodynamic effects for three-dimensional flows using scaling analysis. In the Appendix, we consider rotation-translation coupling of nonconforming contacts coated with a thin compressible elastic layer. A poroelastic material is composed of an elastic solid skeleton and an interstitial fluid. In the general case, where the fluid is free to flow relative to the solid, a composite material cannot be both poroelastic and incompressible.

pressible elastic layer. If the gap profile prior to elastic deformation is parabolic in the vicinity of the contact, the contact is nonconforming. However, if a parabolic description prior to the deformation is insufficient we refer to the contact as conforming, e.g., the degenerate case considered in Sec. IV. Section V treats normal-tangential coupling of nonconforming contacts coated with a thick compressible elastic layer. In Sec. VI, we consider the normal-tangential coupling of nonconforming contacts coated with an incompressible elastic layer. In Sec. VII, we treat the normal-tangential coupling of nonconforming contacts coated with a thin compressible poroelastic layer which describes a biphasic material composed of an elastic solid matrix and a viscous fluid.[27] In Sec. VIII, we study the normal-tangential coupling of a nonconforming contact where one solid is rigid and the other is a deformable cylindrical shell. In Sec. IX, we study a conforming contact: a journal bearing coated with a thin compressible elastic layer. Finally, in Sec. X, we treat the elastohydrodynamics of three-dimensional flows using scaling analysis. Figure 2 provides an overview of the different geometries and elastic materials considered. In the Appendix, we study the coupling between rotation and translation in a soft contact and uncover an elastohydrodynamic analog of the reciprocal theorem for viscous flow.

Our detailed study of a variety of seemingly distinct physical systems allows us to clearly observe their similarities and outline a robust set of features, which we expect to see in any soft contact. In all the cases studied, the normal force=contact area$\times$characteristic hydrodynamic pressure $\times L(\eta)$, where $L(\eta)$ is the dimensionless lift and the softness parameter η=(hydrodynamic pressure/elastic stiffness)f(geometry)=elastic surface displacement/characteristic gap thickness. Tables I and II summarize our results for $\eta \ll 1$. Increasing η increases the asymmetry of the gap profile which results in a repulsive elastohydrodynamic force, i.e., in the generation of lift forces. However, increasing η also decreases the magnitude of the pressure distribution. The competition between symmetry breaking, which dominates for small η, and decreasing pressure, dominant at large η, produces an optimal combination of geometric and material parameters that maximizes the dimensionless lift. Whether or not the dimensional lift has a maximum depends on the control parameter: the normal force increases monotonically with the velocity, but has a maximum as a function of the effective elastic modulus of the system. This suggests that a judicious choice of material may aid in the generation of repulsive elastohydrodynamic forces thereby reducing friction and wear.

II. FLUID LUBRICATION THEORY

We consider a cylinder of radius R moving at a velocity V, rotating with angular frequency ω, and immersed completely in a fluid of viscosity μ and density ρ as shown in Fig. 1. The surfaces are separated by a distance $h(x)$, the gap profile, where the x direction is parallel to the solid surface in the direction of motion and the z direction is perpendicular to the solid surface. We assume that the velocity and pressure field are two dimensional and in the region of contact we use a parabolic approximation, valid for all nonconforming contacts, for the shape of the cylindrical surface in the absence of any elastic deformation. Then the total gap between the cylinder and the solid is given by

TABLE I. Summary of results for two-dimensional flows with small surface deflections.

Geometry	Material	Surface displacement	Lift force/unit length
Thin layer	Compressible elastic solid	$\sqrt{2}\frac{\mu V}{2G+\lambda}\frac{H_l R^{1/2}}{h_0^{3/2}}$	$\frac{3\sqrt{2}\pi}{4}\frac{\mu^2 V^2}{2G+\lambda}\frac{H_l R^{3/2}}{h_0^{7/2}}$
Thin layer with degenerate contact[a]	Compressible elastic solid	$\frac{\mu V}{2G+\lambda}\frac{H_l R^{3/4}}{h_0^{7/4}}$	$\frac{351\pi}{784\sqrt{2}}\frac{\mu^2 V^2}{2G+\lambda}\frac{H_l R^{9/4}}{h_0^{17/4}}$
		$\frac{\mu V}{2G+\lambda}\frac{H_l R^{5/6}}{h_0^{11/6}}$	$0.8859\frac{\mu^2 V^2}{2G+\lambda}\frac{H_l R^{5/2}}{h_0^{9/2}}$
Soft slider	Elastic solid	$\frac{1}{2\pi}\frac{\mu V(\lambda+2G)}{G(\lambda+G)}\frac{R}{h_0}$	$\frac{3\pi^2}{8}\frac{\mu^2 V^2(\lambda+2G)}{G(\lambda+G)}\frac{R^2}{h_0^3}$
Thickness $\sim\sqrt{Rh_0}$	Incompressible elastic solid	$\frac{1}{2\pi}\frac{\mu V}{G}\frac{R}{h_0}$	$\frac{C_i(\zeta)}{2\pi}\frac{\mu^2 V^2}{G}\frac{R^2}{h_0^3}$
Thin layer	Poroelastic	$\sqrt{2}(1-\alpha)\frac{\mu V}{2G+\lambda}\frac{H_l R^{1/2}}{h_0^{3/2}}$	$C_p(\gamma)(1-\alpha)\frac{\mu^2 V^2}{2G+\lambda}\frac{H_l R^{3/2}}{h_0^{7/2}}$
Cylindrical shell	Elastic solid	$3\sqrt{2}\pi^2\frac{\mu V(\lambda+2G)}{G(\lambda+G)}\frac{R^{7/2}}{h_s^3 h_0^{1/2}}$	$6\sqrt{2}\pi^2 C_s\left(\frac{h_0}{R}\right)\frac{\mu^2 V^2(\lambda+2G)}{G(\lambda+G)}\frac{R^{9/2}}{h_s^3 h_0^{5/2}}$
Journal bearing thin layer	Elastic solid	$\frac{H_l \mu R^2 \omega}{h_0^2(2G+\lambda)}$	$C_j(\epsilon_x)\frac{\mu\omega^2 R^2}{2G+\lambda}\frac{H_l R^3}{h_0^5}$

[a]Upper row corresponds to $n=2$, while the lower row corresponds to $n=3$ and the undeformed dimensionless gap thickness profile is $h=1+x^{2n}$.

$$h(x) = h_0\left(1+\frac{x^2}{2h_0R}\right) + H(x), \tag{1}$$

with H being the additional elastic deformation and h_0 the characteristic gap thickness in the absence of the solid deformation. The size of the contact zone, $l_c=\sqrt{2h_0R}$, characterizes the horizontal size over which the lubrication forces are important, consistent with the parabolic approximation in (1). If $h_0 \ll R$, the gap Reynolds number $\mathrm{Re}_g = (\rho V^2/l_c)/(\mu V/h_0^2) \sim \rho V h_0^{3/2}/\mu R^{1/2} \ll \rho VR/\mu = \mathrm{Re}$, the nominal Reynolds number. Then, if $\mathrm{Re}_g \ll 1$, we can neglect the inertial terms and use the lubrication approximation[2] to describe the hydrodynamics. For a two-dimensional velocity field $\mathbf{v}=[v_x(x,z), v_z(x,z)]$ and a pressure field $p(x,z)$, the fluid stress tensor is

$$\boldsymbol{\sigma}_f = \mu(\boldsymbol{\nabla}\mathbf{v} + \boldsymbol{\nabla}\mathbf{v}^T) - p\mathbf{I}. \tag{2}$$

Stress balance in the fluid, $\nabla\cdot\boldsymbol{\sigma}_\mathbf{f}=0$, yields

$$\begin{aligned} 0 &= \partial_z p, \\ 0 &= -\partial_x p + \mu\partial_{zz} v_x. \end{aligned} \tag{3}$$

Mass conservation implies

$$0 = \partial_x v_x + \partial_z v_z. \tag{4}$$

The associated boundary conditions are

$$\begin{aligned} &v_x|_{z=-H} = -V, \quad v_x|_{z=h_0+(x^2/2R)} = -\omega R, \\ &v_z|_{z=-H} = V\partial_x H, \quad v_z|_{z=h_0+(x^2/2R)} = -x\omega, \\ &p|_{x\to\infty} = 0, \quad p|_{x\to-\infty} = 0, \end{aligned} \tag{5}$$

where we have chosen to work in a reference frame translating with the cylinder. We note that the boundary conditions (5) assume that the elastic layer is impermeable to fluid. We make the variables dimensionless with the following definitions:

TABLE II. Summary of results for three-dimensional flows with small surface deflections.

Geometry	Material	Lift force
Thin layer	Compressible elastic solid	$\frac{\mu^2 V^2}{2G+\lambda}\frac{H_l R^2}{h_0^3}$
Thin layer with degenerate contact	Compressible elastic solid	$\frac{\mu^2 V^2}{2G+\lambda}\frac{H_l R^{4-(2/n)}}{h_0^{5-(2/n)}}$
Soft slider	Elastic solid	$\frac{\mu^2 V^2}{G}\frac{R^{5/2}}{h_0^{5/2}}$
Thickness $\gtrsim\sqrt{Rh_0}$	Incompressible elastic solid	$\frac{\mu^2 V^2}{G}\frac{R^{5/2}}{h_0^{5/2}}$
Thickness $\ll\sqrt{Rh_0}$	Incompressible elastic solid	$\frac{\mu^2 V^2}{G}\frac{H_l R^{3/2}}{h_0^{5/2}}$
Thin layer	Poroelastic	$\frac{\mu^2 V^2}{2G+\lambda}\frac{H_l R^2}{h_0^3}$
Cylindrical shell $h_s \gg h_0$	Elastic solid	$\frac{\mu^2 V^2}{G}\frac{R^4}{h_s^{5/2}h_0^{3/2}}$
Cylindrical shell $h_s \lesssim h_0$	Elastic solid	$\frac{\mu^2 V^2}{G}\frac{R^{5/2}}{h_s h_0^{3/2}}$
Journal bearing thin layer	Elastic solid	$\frac{\mu\omega^2 R^2}{2G+\lambda}\frac{H_l R^4}{h_0^5}$

$$x = l_c x', \quad z = h_0 z', \quad p = p_0 p' = \frac{l_c \mu (V-\omega R)}{h_0^2} p',$$

$$\boldsymbol{\sigma}_f = p_0 \boldsymbol{\sigma}_f' = \frac{l_c \mu (V-\omega R)}{h_0^2}\boldsymbol{\sigma}_f', \quad h = h_0 h', \quad H = H_0 H', \tag{6}$$

$$v_x = (V-\omega R)v_x', \quad v_z = \frac{(V-\omega R)h_0}{l_c} v_z'.$$

Here, $H_0(p_0/E', l_2/l_1, l_3/l_1, \ldots)$ is the characteristic scale of the deflection, where E' is the effective elastic modulus of the medium and l_i are the length scales of the system. The pressure scaling follows from (3) and the fact that $x \sim l_c = \sqrt{2h_0 R}$, the size of the contact zone. Then, after dropping the primes the dimensionless versions of Eqs. (3)–(5) are

$$0 = \partial_z p,$$

$$0 = -\partial_x p + \partial_{zz} v_x,$$

$$0 = \partial_x v_x + \partial_z v_z,$$

$$v_x|_{z=-\eta H} = \frac{-1}{1-\omega'}, \quad v_x|_{z=1+x^2} = \frac{-\omega'}{1-\omega'}, \tag{7}$$

$$v_z|_{z=-\eta H} = \frac{\eta \partial_x H}{1-\omega'}, \quad v_z|_{z=1+x^2} = \frac{-2x\omega'}{1-\omega'}.$$

$$p|_{x\to\infty} = 0, \quad p|_{x\to-\infty} = 0.$$

Here $\omega' = \omega R/V$ characterizes the ratio of rolling to sliding, the softness parameter, $\eta = H_0/h_0$, characterizes the scale of the elastic deformation relative to the gap thickness, which is related to the compliance of the elastic material. The dimensionless version of the fluid stress tensor (2) is

$$\boldsymbol{\sigma}_f = \begin{pmatrix} -p + 2\varepsilon^2 \partial_x v_x & \varepsilon \partial_z v_x + \varepsilon^3 \partial_x v_z \\ \varepsilon \partial_z v_x + \varepsilon^3 \partial_x v_z & -p + 2\varepsilon^2 \partial_z v_z \end{pmatrix}, \tag{8}$$

where $\varepsilon = \sqrt{h_0/2R}$. Solving (7) gives the Reynolds equation[28]

$$0 = \partial_x (6h + h^3 \partial_x p), \tag{9}$$

subject to

$$p(\infty) = p(-\infty) = 0. \tag{10}$$

Note that ω' is scaled away. Here, h is the gap profile given by (1) in dimensionless terms

$$h(x) = 1 + x^2 + \eta H(x). \tag{11}$$

To close the system we need to determine $\eta H(x)$, the elastic response to the hydrodynamic forces. This depends on the detailed geometry and constitutive behavior of the cylindrical contact. In the following sections, we explore various configurations that allow us to explicitly calculate ηH, thus allowing us to calculate the normal force on the cylinder,

$$L = \int_{\text{contact area}} p dA, \tag{12}$$

and determine the elastohydrodynamic tangential-normal coupling. We note that when $\eta = 0$, the contact is symmetric (11) so that the form of (9) implies that $p(-x) = -p(x)$ and $L = 0$.

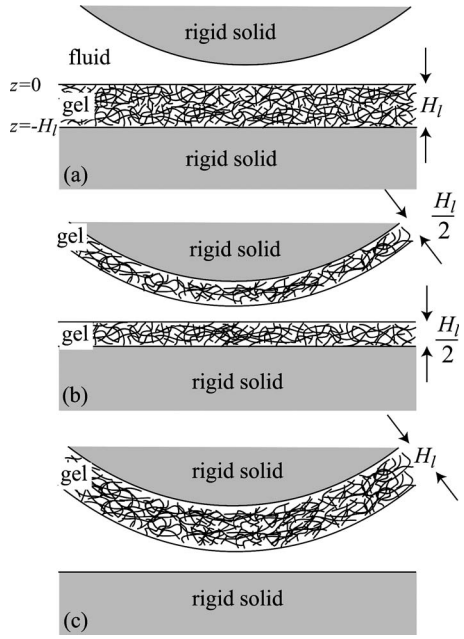

FIG. 3. Schematic diagrams of mathematically identical configurations. Configuration (a) is treated in the text.

III. ELASTIC "LUBRICATION" THEORY: DEFORMATION OF A THIN ELASTIC LAYER

In our first case, we consider a thin elastic layer of thickness H_l coating the cylinder or the rigid wall or both, all of which are mathematically equivalent (Fig. 3). Our descrip-

tion of the layer as thin means that the layer is thin compared to other length scales in the problem such as the contact length l_c. The layer thickness H_l is smaller than the length scale of the hydrodynamic contact zone, $l_c=\sqrt{2h_0R}$, i.e., $H_l \ll l_c$. We first turn our attention to determine the surface deflection of the layer for an arbitrary applied traction. Throughout the analysis, we assume that the surface deflection $H_0 \ll H_l$ so that a linear elastic theory suffices to describe the material response. The stress tensor $\boldsymbol{\sigma}_s$ for a linearly elastic isotropic material with Lamé coefficients G and λ is

$$\boldsymbol{\sigma}_s = G(\boldsymbol{\nabla}\mathbf{u} + \boldsymbol{\nabla}\mathbf{u}^T) + \lambda\,\boldsymbol{\nabla}\cdot\mathbf{u}\mathbf{I}, \tag{13}$$

where $\mathbf{u}=(u_x,u_z)$ is the displacement field and $\mathbf{I}$ is the identity tensor. Stress balance in the solid implies

$$\boldsymbol{\nabla}\cdot\boldsymbol{\sigma}_s = 0. \tag{14}$$

We make the equations dimensionless using

$$z = H_l z', \quad x = l_c x', \quad u_x = h_0 u_x', \quad u_z = h_0 u_z' \quad \boldsymbol{\sigma}_s = p_0 \boldsymbol{\sigma}_s'. \tag{15}$$

We note that the length scale in the z direction is the depth of the layer H_l; the length scale in the x direction is the length scale of the hydrodynamic contact zone, $l_c=\sqrt{2h_0R}$; the displacements u_x and u_z have been scaled with the characteristic gap thickness h_0; and the stress has been scaled using the hydrodynamic pressure scale following (6). We take the thickness of the solid layer to be small compared to the length scale of the contact zone with $\zeta=H_l/l_c \ll 1$ and restrict our attention to compressible elastic materials, where $G\sim\lambda$. Then, after dropping primes, the dimensionless two-dimensional form of the stress tensor (13) is

$$\boldsymbol{\sigma}_s = \frac{1}{\eta}\begin{pmatrix} \dfrac{\lambda}{2G+\lambda}\partial_z u_z + \zeta\partial_x u_x & \dfrac{G}{2G+\lambda}\partial_z u_x + \zeta\dfrac{G}{2G+\lambda}\partial_x u_z \\ \dfrac{G}{2G+\lambda}\partial_z u_x + \zeta\dfrac{G}{2G+\lambda}\partial_x u_z & \partial_z u_z + \zeta\dfrac{\lambda}{2G+\lambda}\partial_x u_x \end{pmatrix}. \tag{16}$$

Here,

$$\eta = \frac{p_0}{2G+\lambda}\frac{H_l}{h_0} = \sqrt{2}\frac{\mu(V-\omega R)}{2G+\lambda}\frac{H_l R^{1/2}}{h_0^{5/2}} \tag{17}$$

is the softness parameter, a dimensionless number governing the relative size of the surface deflection to the undeformed gap thickness. Stress balance (14) yields

$$\begin{aligned} &\partial_{zz}u_x + \zeta\left(1+\frac{\lambda}{G}\right)\partial_{xz}u_z + \zeta^2\left(2+\frac{\lambda}{G}\right)\partial_{xx}u_x = 0, \\ &\partial_{zz}u_z + \zeta\frac{G+\lambda}{2G+\lambda}\partial_{xz}u_x + \zeta^2\frac{G}{2G+\lambda}\partial_{xx}u_z = 0, \end{aligned} \tag{18}$$

so that to $O(\zeta)$ the leading order balance is

$$\partial_{zz}u_x = 0, \quad \partial_{zz}u_z = 0. \tag{19}$$

The normal unit vector to the soft interface is $\mathbf{n}=(-\partial_x u_z|_{z=0},1)$, which in dimensionless form is

$$\mathbf{n} = (-\varepsilon\partial_x u_z|_{z=0},1), \tag{20}$$

where $\varepsilon=\sqrt{h_0/2R}$. The balance of normal traction on the solid-fluid interface yields

$$\boldsymbol{\sigma}_f\cdot\mathbf{n}|_{z=0} = \boldsymbol{\sigma}_s\cdot\mathbf{n}|_{z=0}, \tag{21}$$

so that

$$\partial_z u_x|_{z=0} = 0, \quad \partial_z u_z|_{z=0} = -\eta p. \tag{22}$$

At the interface between the soft film and the rigid substrate, the no-slip condition yields

$$u_z(x,-1) = 0, \quad u_x(x,-1) = 0. \tag{23}$$

Solving (19), (22), and (23) gives us the displacement of the solid-fluid interface

$$u_x(x,0) = 0, \quad u_z(x,0) = -\eta p = -\eta H(x). \tag{24}$$

This linear relationship between the normal displacement and fluid pressure is known as the Winkler or "mattress" elastic foundation model.[29] In light of (24), we may write the gap profile (11) as

$$h = 1 + x^2 + \eta p. \tag{25}$$

Equations (9), (10), and (25) form a closed system for the elastohydrodynamic response of a thin elastic layer coating a rigid cylinder. We note that Lighthill[13] found a similar set of equations while studying the flow of a red blood cell through a capillary. However, his model's axisymmetry proscribed the existence of a force normal to the flow.

When $\eta \ll 1$, we can employ a perturbation analysis to find the lift force experienced by the cylinder. We use an expansion of the form

$$p = p^{(0)} + \eta p^{(1)} + O(\eta^2), \quad h = h^{(0)} + \eta h^{(1)} + O(\eta^2), \tag{26}$$

to find

$$\eta^0: \partial_x\{6h^{(0)} + [h^{(0)}]^3\partial_x p^{(0)}\} = 0, \tag{27}$$

$$\eta^1: \partial_x\{6h^{(1)} + 3[h^{(0)}]^2 h^{(1)}\partial_x p^{(0)} + [h^{(0)}]^3\partial_x p^{(1)}\} = 0, \tag{28}$$

where

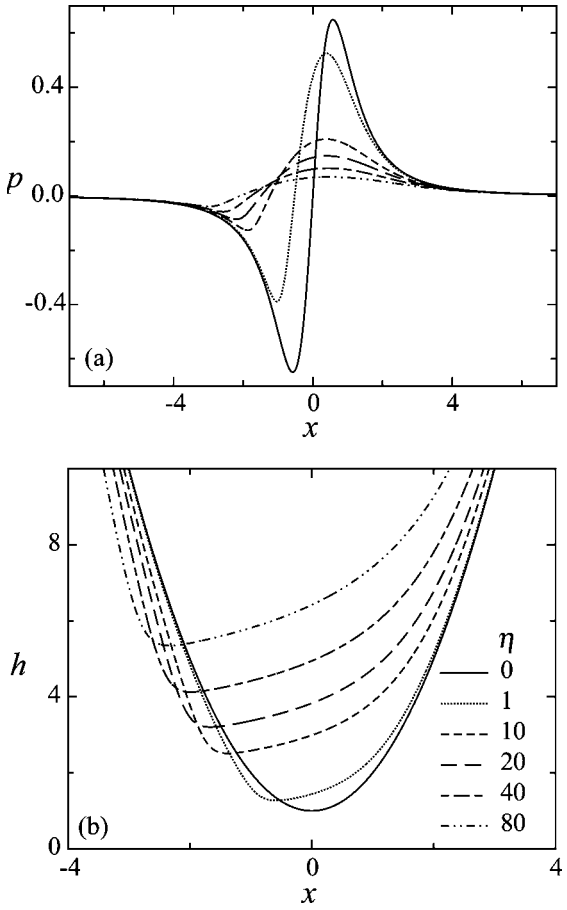

FIG. 4. (a) Pressure $p(x)$ as a function of η. (b) Gap thickness profile $h(x)=1+x^2+\eta p$ as a function of η. The symmetry of the initially parabolic gap thickness profile is broken and the maximum value of the pressure decreases as η increases.

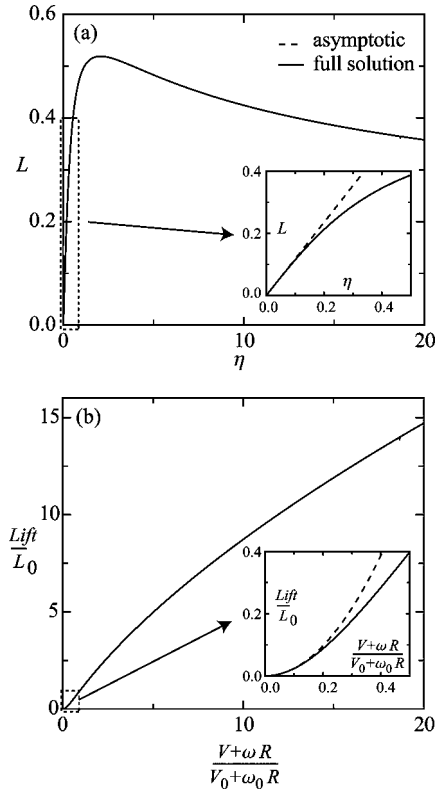

FIG. 5. (a) Dimensionless lift per unit length L plotted against η, the softness parameter. L has a maximum at $\eta=2.06$ which is the result of a competition between symmetry breaking (dominant for $\eta \ll 1$) and decreasing pressure (dominant for $\eta \gg 1$) due to increasing the gap thickness. For small η asymptotic analysis yields $L=(3\pi/8)\eta$, which matches the numerical solution. (b) The dimensional lift force, *Lift*, is quadratic in the velocity for small velocities while being roughly linear for large velocities. $V_0+\omega_0 R=[h_0^{5/2}(2G+\lambda)/\sqrt{2RH_l\mu}]$ is the velocity and rate of rotation at which $\eta=1$, and L_0 is corresponding lift.

$$h^{(0)}=1+x^2, \quad h^{(1)}=p^{(0)}, \tag{29}$$

subject to the boundary conditions

$$p^{(0)}(\infty)=p^{(0)}(-\infty)=p^{(1)}(\infty)=p^{(1)}(-\infty)=0. \tag{30}$$

Solving (27)–(30) yields

$$p=\frac{2x}{(1+x^2)^2}+\eta\frac{3(3-5x^2)}{5(1+x^2)^5}+O(\eta^2), \tag{31}$$

so that

$$L=\int p\,dx=\frac{3\pi}{8}\eta. \tag{32}$$

In dimensional form, the lift force per unit length is

$$L=\frac{3\sqrt{2}\pi}{8}\frac{p_0^2}{2G+\lambda}\frac{H_l\sqrt{R}}{\sqrt{h_0}}=\frac{3\sqrt{2}\pi}{4}\frac{\mu^2(V-\omega R)^2}{2G+\lambda}\frac{H_l R^{3/2}}{h_0^{7/2}}, \tag{33}$$

as reported in Ref. 30. The same scaling was found in Ref. 22 but with a different prefactor owing to a typographical error. When $\eta=O(1)$, the system (9), (10), and (25) is solved numerically using a continuation method[31] with η as the continuation parameter. In Fig. 4, we show the pressure distribution $p(x)$ and the gap $h(x)$ as a function of η. For $\eta \ll 1$, $p(-9\eta/10)=0$. As η increases, h increases and the asymmetric gap profile begins to resemble that of a tilted slider bearing, which is well known to generate lift forces. However, an increase in the gap thickness also decreases the peak pressure $\sim \mu V R^{1/2}/h_0^{3/2}$ [see Fig. 4(a)]. The competition between symmetry breaking, dominant for $\eta \lesssim 1$, and decreasing pressure, dominant for $\eta \gtrsim 1$, produces a maximum scaled lift force at $\eta=2.06$. In dimensional terms, this implies that the lift as a function of the effective modulus $2G+\lambda$ will have a maximum, however, the lift as a function of the relative motion between the two surfaces $V-\omega R$ increases monotonically [see Fig. 5(b)]. In fact, (33) shows that the dimensional lift increases as $(V-\omega R)^2$ for $\eta \ll 1$.

IV. DEGENERATE CONTACT

In this section, we consider the case where the parabolic approximation in the vicinity of the contact breaks down. Since rotation changes the nature of the contact region for such interfaces, we consider only a purely sliding motion with $\omega=0$. We assume that the gap thickness is described by

$$h = h_0\left(1 + \frac{x^{2n}}{h_0 R^{2n-1}}\right) + H(x), \tag{34}$$

where $n=2,3,\ldots$ characterizes the geometric nature of the contact and the contact length is $l_c \sim (h_0 R^{2n-1})^{1/2n}$. We note that we always focus on symmetric contacts. We make the variables dimensionless using the following scalings:

$$h = h_0 h', \quad x = l^* x' = h_0^{1/2n} R^{1-1/2n} x',$$
$$p = p^* p' = \mu V \frac{R^{1-1/2n}}{h_0^{2-1/2n}} p'. \tag{35}$$

In Sec. III, we have seen that for a thin compressible soft layer the pressure and surface deflection can be linearly related by (24) so that the scale of the deflection is $h_0\eta = p_0 H_l/(2G+\lambda)$. To find the scale of the deflection for the degenerate contact described by (34), we replace p_0 with the appropriate pressure scale p^*, so that

$$H = \frac{p^*}{2G+\lambda} H_l H' = \frac{\mu V}{2G+\lambda} \frac{H_l R^{1-1/2n}}{h_0^{2-1/2n}}, \tag{36}$$

and the size of the deformation relative to the gap size is governed by the dimensionless group

$$\eta = \frac{p^*}{2G+\lambda}\frac{H_l}{h_0} = \frac{\mu V}{2G+\lambda}\frac{H_l R^{1-1/2n}}{h_0^{3-1/2n}}. \tag{37}$$

Then the dimensionless version of the gap thickness profile (34) is

$$h = 1 + x^{2n} + \eta p. \tag{38}$$

As in Sec. III, we employ a perturbation expansion for the pressure field in the parameter η ($\ll 1$) to solve (9), (10), and (38) and find the pressure field and the lift for small η. This yields $p = p_0 + \eta p_1$ and gives the following dimensionless result:

$$L_{n=2} = \frac{351\pi}{784\sqrt{2}}\eta, \quad L_{n=3} = 0.8859\eta, \tag{39}$$

where we have not shown the pressure distribution due to its unwieldy size. In dimensional terms, the normal force reads as

$$L_{n=2} = \frac{351\pi}{784\sqrt{2}}\frac{p^{*2}}{2G+\lambda}\frac{H_l l^*}{h_0} = \frac{351\pi}{784\sqrt{2}}\frac{\mu^2 V^2 H_l R^{9/4}}{(2G+\lambda)h_0^{17/4}}, \tag{40}$$

$$L_{n=3} = 0.8859\frac{p^{*2}}{2G+\lambda}\frac{H_l l^*}{h_0} = 0.8859\frac{\mu^2 V^2 H_l R^{5/2}}{(2G+\lambda)h_0^{9/2}}. \tag{41}$$

The results for $n=2$ and $n=3$ are shown in Figs. 6 and 7. One noteworthy feature of a degenerate contact is that the torque

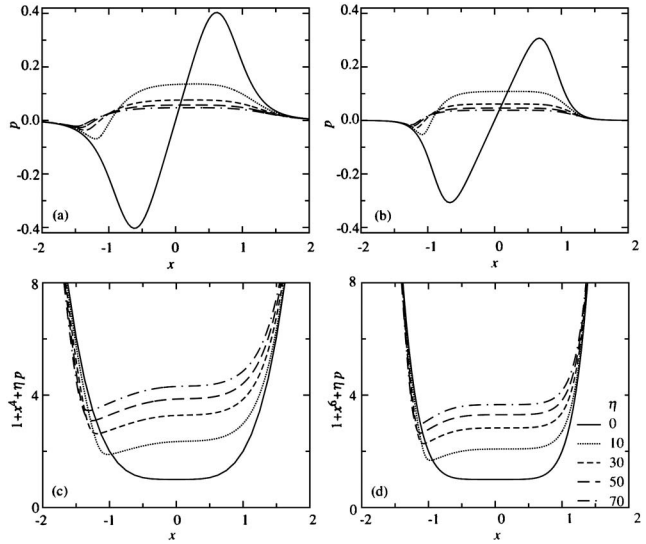

FIG. 6. Pressure distribution and gap thickness profile for degenerate contacts corresponding to a gap thickness profile of $h=1+x^{2n}+\eta p$ with $n=2$ (a) and (c), and $n=3$ (b) and (d).

experienced by the slider arises from the fluid pressure rather than the shear force because the normal to the surface no longer passes through the center of the object as it would for a cylinder or sphere. The ratio of the torque due to the shear to the torque due to the pressure is

$$\frac{\text{shear torque}}{\text{pressure torque}} \sim \frac{\mu V R/h_0}{p l_c} \sim \left(\frac{h_0}{R}\right)^{1-1/n} \ll 1, \tag{42}$$

provided $n>1$ as for degenerate contacts. Hence, the dominant contribution to the torque is due to the pressure and

$$\Gamma = \int p x dA. \tag{43}$$

For $\eta \ll 1$, $p = p_0 + O(\eta)$ so that

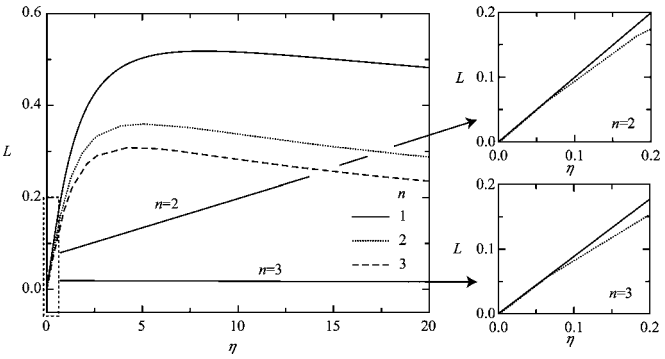

FIG. 7. Dimensionless lift for $h=1+x^{2n}+\eta p$ where $n=1,2,3$. The curves are similar, however, they cannot be rescaled to a universal curve.

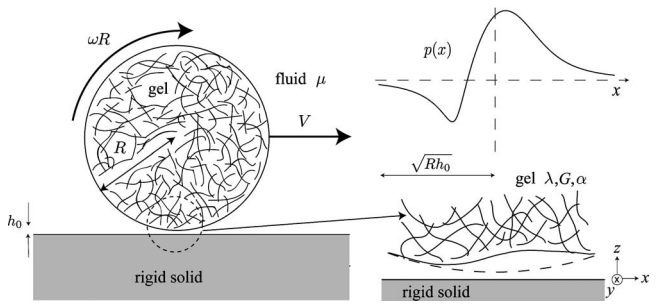

FIG. 8. Schematic diagram of a gel cylinder moving through a liquid over a rigid solid substrate. The asymmetric pressure distribution pushes on the gel when the fluid pressure in the gap is positive while pulling on the gel when the pressure is negative. This breaks the symmetry of the gap thickness profile $h(x)$ and gives rise to a repulsive force of elastohydrodynamic origin. The dashed line in the lower right hand denotes the undeformed location of the gel cylinder.

$$
\begin{aligned}
n = 2{:}p_0 &= \frac{6x}{7(1+x^4)^2}, \quad \Gamma = \frac{3\pi}{14\sqrt{2}}, \\
n = 3{:}p_0 &= \frac{6x}{11(1+x^6)^2}, \quad \Gamma = \frac{\pi}{11}, \\
n = m{:}p_0 &= \frac{6x}{(4m-1)(1+x^{2m})^2}, \\
\Gamma &= \frac{3\pi(2m-3)\csc\dfrac{3\pi}{2m}}{m^2(4m-1)}.
\end{aligned}
\tag{44}
$$

V. SOFT SLIDER

To contrast our result for a soft thin layer with that for a soft slider, we consider the case where the entire cylindrical slider of length $2l$ and radius R is made of a soft material with Lamé coefficients G and λ. Equivalently, we could have a rigid slider moving above a soft semi-infinite half space. Since the deformation is no longer locally determined by the pressure, we use a Green's function approach to determine the response to the hydrodynamic pressure. We note that we have considered a cylinder of finite length in the direction perpendicular to the flow, rather than the apparently simpler two-dimensional case, in order to avoid a logarithmic divergence in the deformation. Following Ref. 32, we use the Green's function for a point force on a half space since the scale of the contact zone, $l_c \sim \sqrt{h_0 R} \ll R$, the cylinder radius. Deformation at the surface due to a pressure field $p(x,y)$ will be[33]

$$
H(x,y) = \frac{\lambda + 2G}{4\pi G(\lambda + G)} \int \frac{p(x',y')dx'\,dy'}{\sqrt{(x'-x)^2 + (y'-y)^2}}, \tag{45}
$$

with x, y as defined in Fig. 8. Neglecting the end effects, so that the pressure is a function of x only, we integrate (45) over y' to get

$$
\begin{aligned}
H(x,y) &= \frac{\lambda + 2G}{4\pi G(\lambda + G)} \\
&\quad \times \int_{-\infty}^{\infty} \left[p(x') \int_{-l}^{l} \frac{dy'}{\sqrt{(x'-x)^2 + (y'-y)^2}} \right] dx' \\
&= \frac{\lambda + 2G}{4\pi G(\lambda + G)} \int_{-\infty}^{\infty} \log\left[\frac{4(l^2 - y^2)}{(x-x')^2} \right] p(x')dx'.
\end{aligned}
\tag{46}
$$

To make the equations dimensionless, we employ the following scalings:

$$
\begin{aligned}
&x = \sqrt{2h_0 R}\,x', \quad y = ly', \quad h = h_0 h', \\
&H = h_0 H', \quad p = p_0 p' = \frac{\sqrt{2R}\mu(V - \omega R)}{h_0^{3/2}} p',
\end{aligned}
\tag{47}
$$

so that the dimensionless gap thickness (11) now reads

$$
h = 1 + x^2 + \eta \int_{-\infty}^{\infty} dx' p(x') \log\left[\frac{Y}{(x-x')^2} \right], \tag{48}
$$

where

$$
\eta = \frac{1}{2\pi} \frac{\mu(V - \omega R)(\lambda + 2G)}{G(\lambda + G)} \frac{R}{h_0^2}, \quad Y = \frac{2l^2}{Rh_0}(1 - y^2). \tag{49}
$$

Comparing with our softness parameter for a thin section, we see that

$$
\frac{\eta_{\text{thin layer}}}{\eta_{\text{soft slider}}} = 2\pi\sqrt{2} \frac{G(G+\lambda)}{(2G+\lambda)^2} \frac{H_l}{\sqrt{h_0 R}} \sim \frac{H_l}{\sqrt{h_0 R}} \ll 1, \tag{50}
$$

i.e., a thin layer is stiffer than a half space made from the same material by the geometric factor $\sqrt{h_0 R}/H_l$. For small η we write $p = p_0 + \eta p_1$, where $p_0 = 2x/(1+x^2)^2$ as in (31). Substituting into (48) yields

$$
h = 1 + x^2 + \eta \frac{2\pi x}{1 + x^2} + O(\eta^2). \tag{51}
$$

To order η, (9) and (10) yield the equations for the perturbation pressure p_1,

$$
\begin{aligned}
&\eta : 0 = \partial_x \left[(1+x^2)^3 \partial_x p_1 + \frac{24\pi x(x^2-1)}{(1+x^2)^2} \right], \\
&p_1(-\infty) = p_1(\infty) = 0,
\end{aligned}
\tag{52}
$$

which has the solution

$$
p_1 = \frac{2\pi(2x^2 - 1)}{(1+x^2)^4}. \tag{53}
$$

Hence the dimensionless lift force is

$$
L = \eta \int p_1 dx = \eta \int \frac{2\pi(2x^2-1)}{(1+x^2)^4} dx = \frac{3\pi^2}{8}\eta. \tag{54}
$$

In dimensional terms, the lift force is

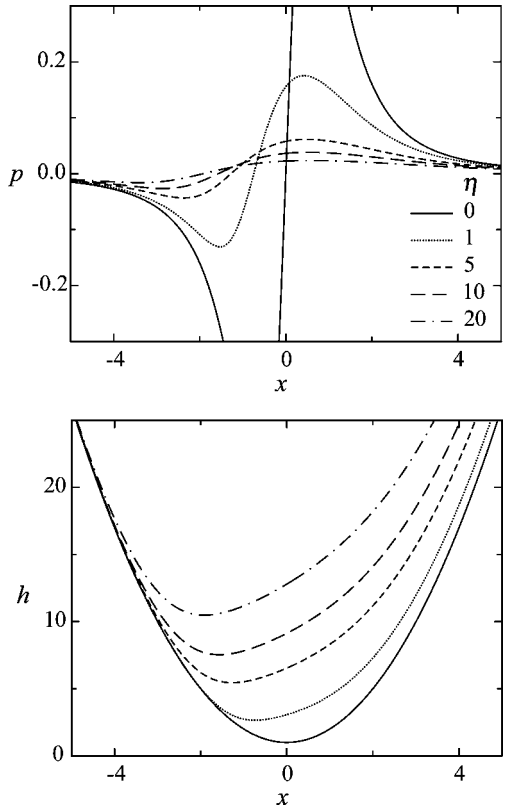

FIG. 9. Gap thickness h and pressure p as a function of η for a soft cylindrical gel slider. We note that while the pressure distribution is localized to the region near the point of closest contact, the change in gap thickness is spread out due to the logarithmic nature of the Green's function of a line contact: $h=1+x^2+\eta\int dx' p(x')\log[Y/(x-x')^2]$.

$$L=\frac{3\pi}{8}\frac{\mu^2(V-\omega R)^2(\lambda+2G)}{G(\lambda+G)}\frac{R^2}{h_0^3}. \tag{55}$$

Comparing this expression with that for the case of a thin elastic layer, Eq. (33), we see that confinement acts to reduce the deformation and hence reduce the lift in the small deflection, $\eta\ll 1$, regime. When $\eta=O(1)$, we solve (9), (10), and (48) for $p(x)$ using an iterative procedure. First, we guess an initial gap profile h_{old} and use a shooting algorithm to calculate the pressure distribution. The new pressure distribution is then used in Eq. (48) with $Y=1000$ (corresponding to a very long cylinder) to calculate a new gap profile, h_{new}. If $\int_{-10}^{10}(h_{\text{old}}-h_{\text{new}})^2dx<10^{-6}$ the calculation is stopped, else we set $h_{\text{old}}=h_{\text{new}}$ and iterate. The results are shown in Figs. 9 and 10, and not surprisingly they have the same qualitative features discussed previously, i.e., for $\eta\ll 1$, $L\sim\eta$; L shows a maximum at $\eta=0.25$ and decreases when $\eta>0.25$. The reasons for this are the same as before, i.e., the competing effects of an increase in the gap thickness and the increased asymmetry of the contact zone.

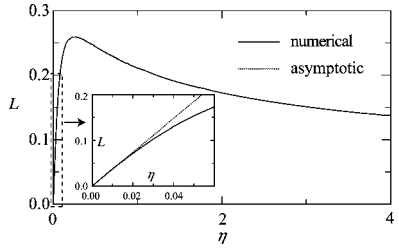

FIG. 10. Dimensionless lift as a function of η a measure of the increase in gap thickness for a soft cylindrical gel slider. For $\eta\ll 1$, $L=(3\pi^2/8)\eta$.

VI. INCOMPRESSIBLE LAYER

In contrast to compressible layers, an incompressible layer (e.g., one made of an elastomer) can deform only via shear. For thin layers, incompressibility leads to a geometric stiffening.[29] To address this problem in the most general case, we use a Green's function approach. The constitutive behavior for an incompressible linearly elastic solid is

$$\boldsymbol{\sigma}=G(\nabla\mathbf{u}+\nabla\mathbf{u}^T)-p_s\mathbf{I}, \tag{56}$$

where $\mathbf{u}=(u_x,u_y,u_z)$ is the displacement and p_s is the pressure in the solid. Mechanical equilibrium in the solid implies $\nabla\cdot\boldsymbol{\sigma}=0$, i.e.,

$$\begin{aligned}0&=-\partial_x p_s+G\nabla^2u_x,\\ 0&=-\partial_y p_s+G\nabla^2u_y,\\ 0&=-\partial_z p_s+G\nabla^2u_z.\end{aligned} \tag{57}$$

Incompressibility of the solid implies

$$0=\nabla\cdot\mathbf{u}=\partial_x u_x+\partial_y u_y+\partial_z u_z. \tag{58}$$

For the Green's function associated with a point force, $\sigma_{zz}|_{z=0}=-f\delta(x)\delta(y)$, where δ is a delta function, the boundary conditions are

$$\begin{aligned}&u_x=u_y=u_z=0 \quad \text{at } z=-H_l,\\ &\sigma_{xz}=\sigma_{xy}=0 \quad \text{at } z=0,\\ &\sigma_{zz}=-f\delta(x)\delta(y) \quad \text{at } z=0.\end{aligned} \tag{59}$$

We solve the boundary value problem (57)–(59) by using a two-dimensional Fourier transforms defined as

$$u_x=\int_{-\infty}^{\infty}\int_{-\infty}^{\infty}\hat{u}_x(k_x,k_y,z)e^{-i(k_xx+k_yy)}dk_xdk_y,\ \ldots\ . \tag{60}$$

Then Eqs. (57)–(59) in Fourier space are

$$\begin{aligned}0&=ik_x\hat{p}_s+G(-k_x^2\hat{u}_x-k_y^2\hat{u}_x+\partial_{zz}\hat{u}_x),\\ 0&=ik_y\hat{p}_s+G(-k_x^2\hat{u}_y-k_y^2\hat{u}_y+\partial_{zz}\hat{u}_y),\\ 0&=-\partial_z\hat{p}_s+G(-k_x^2\hat{u}_z-k_y^2\hat{u}_z+\partial_{zz}\hat{u}_z),\\ 0&=-ik_x\hat{u}_x-ik_y\hat{u}_y+\partial_z\hat{u}_z,\end{aligned} \tag{61}$$

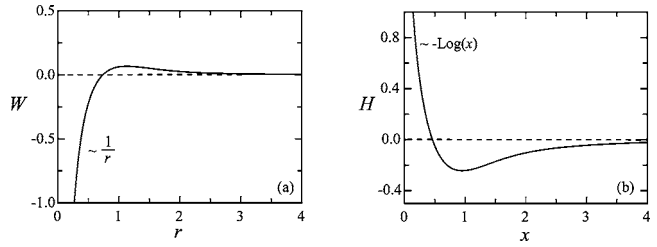

FIG. 11. Green's function for a point force (a) and a line load (b) acting on an incompressible layer of dimensionless thickness $\zeta = H_l/l_c = 1$.

subject to the boundary conditions

$$\begin{aligned}
&\hat{\sigma}_{xz} = 0 = \partial_z \hat{u}_x - ik_x \hat{u}_z \quad \text{at } z = 0,\\
&\hat{\sigma}_{yz} = 0 = \partial_z \hat{u}_y - ik_y \hat{u}_z \quad \text{at } z = 0,\\
&\hat{\sigma}_{zz} = -f = -\hat{p}_s + 2G\partial_z \hat{u}_z \quad \text{at } z = 0,\\
&\hat{u}_x = \hat{u}_y = \hat{u}_z = 0 \quad \text{at } z = -H_l.
\end{aligned} \tag{62}$$

Solving (61) and (62) for $\hat{u}_z(z=0)$, we find

$$\hat{u}_z(k_x,k_y,0) = f\frac{2H_l - \dfrac{\sinh(2H_l\sqrt{k_x^2+k_y^2})}{\sqrt{k_x^2+k_y^2}}}{2G[1+2H_l^2(k_x^2+k_y^2)+\cosh(2H_l\sqrt{k_x^2+k_y^2})]}. \tag{63}$$

Since this corresponds to a radially symmetric integral kernel, we can take $q=\sqrt{k_x^2+k_y^2}$ and use the Hankel transform, $u_z = 1/2\pi\int_0^\infty J_0(rq)q\hat{u}_z dq$, to find the surface displacement,[34]

$$\begin{aligned}
u_z(r)|_{z=0} &= \frac{f}{4\pi G}\int_0^\infty J_0(rq)\frac{2H_l q - \sinh(2H_l q)}{1+2H_l^2 q^2+\cosh(2H_l q)}dq\\
&= \frac{f}{4\pi G H_l}W(r),
\end{aligned} \tag{64}$$

where $r=\sqrt{x^2+y^2}$ and $J_0(rq)$ is a Bessel function of the first kind. To see the form of the surface displacement, we integrate (64) numerically and show the dimensionless function $W(r)$ in Fig. 11(a). The surface displacement H for a pressure distribution $p(x)$ is found using the Green's function for a point force (64), so that

$$H = -\int_{-\infty}^{\infty}\frac{p(x^*)}{4\pi G}\left\{\int_{-\infty}^{\infty}\left[\int_0^\infty J_0(rq)\frac{2H_l q - \sinh 2H_l q}{1+2H_l^2 q^2+\cosh 2H_l q}dq\right]dy^*\right\}dx^*, \tag{65}$$

where $r=\sqrt{(x-x^*)^2+(y-y^*)^2}$. In terms of dimensionless variables with the following definitions:

$$\begin{aligned}
&p = p_0 p', \quad q = \frac{q'}{\sqrt{2h_0 R}}, \quad x = \sqrt{2h_0 R}x', \quad x^* = \sqrt{2h_0 R}x'^*,\\
&y = \sqrt{2h_0 R}y', \quad y^* = \sqrt{2h_0 R}y'^*, \quad r = \sqrt{2h_0 R}r',\\
&h = h_0 h', \quad H = \frac{p_0\sqrt{2h_0 R}}{4\pi G}H' = \frac{\mu(V-\omega R)}{2\pi G}\frac{R}{h_0}H',
\end{aligned} \tag{66}$$

Eq. (65) may be rewritten (after dropping primes) as

$$\begin{aligned}
H = &-\int_{-\infty}^{\infty} p(x^*)\\
&\times\left\{\int_{-\infty}^{\infty}\left[\int_0^\infty J_0(rq)\frac{2\zeta q - \sinh 2\zeta q}{1+2\zeta^2 q^2+\cosh 2\zeta q}dq\right]dy^*\right\}dx^*,
\end{aligned} \tag{67}$$

where $r=\sqrt{(x-x^*)^2+(y-y^*)^2}$ and the dimensionless group $\zeta = H_l/\sqrt{2h_0 R}$ is the ratio of the layer thickness to the size of the contact zone. To understand the form of (67), we consider the response of a line force $p(x^*)=\delta(x^*)$ and show the results graphically in Fig. 11(b). Moving on to the case at hand, that of a parabolic contact of a cylinder of length $2l$, we write the dimensionless gap thickness as

$$h = 1 + x^2 + \eta H,$$

where

$$\eta = \frac{1}{2\sqrt{2}\pi}\frac{p_0}{G}\sqrt{\frac{R}{h_0}} = \frac{1}{2\pi}\frac{\mu(V-\omega R)}{G}\frac{R}{h_0^2}. \tag{68}$$

For $\eta \ll 1$, we can expand the pressure p in powers of η and carry out a perturbation analysis as in Sec. III. This yields a linear relation between the dimensionless lift L and the scale of the deformation: $L = C_i(\zeta)\eta$, where $C_i(\zeta)$ is shown in Fig. 12(d). The dimensional lift per unit length is

$$L = \frac{C_i(\zeta)}{2\pi}\frac{\mu^2(V-\omega R)^2}{G}\frac{R^2}{h_0^3}. \tag{69}$$

As $\zeta \to \infty$, we approach the limit of an infinitely thick layer, in which case there is no stiffening due to incompressibility, so that $C(\zeta) \to 3\pi^2/8$, which is the result for an infinitely thick layer. To study the effects of confinement on a thick layer, i.e., $\zeta \gg 1$, we approximate (67) as

$$\begin{aligned}
H \approx &-\int_{-\infty}^{\infty} p(x^*)\int_{-l'}^{l'}\left\{\int_0^\infty J_0(rq)\right.\\
&\left.\times[1-(2+4\zeta q+\zeta^2 q^2)e^{-2\zeta q}]dq\right\}dy^* dx^*,
\end{aligned} \tag{70}$$

where we are now integrating y^* over the dimensionless

length of the cylinder $l'=l/\sqrt{2h_0R}\gg 1$, since the interactions for deep layers are not limited by confinement effects. Evaluating (70) yields

$$H\approx\int_{-\infty}^{\infty}p(x^*)\times\left\{\int_{-l'}^{l'}\left[-\frac{1}{r}-\frac{2r^4+20r^2\zeta^2+96\zeta^4}{(r^2+4\zeta^2)^{5/2}}\right]dy^*\right\}dx^*. \tag{71}$$

Integrating (71) with respect to y^* and keeping the leading order terms in l' yields

$$H\approx\int_{-\infty}^{\infty}\frac{2x^*}{(1+x^{*2})^2}\left\{\log\left[\frac{4(l'^2-y^2)}{(x-x^*)^2}\right]+2\log\left[\frac{(x-x^*)^2+4\zeta^2}{4(l'^2+y^2)}\right]-\frac{8\zeta^2[(x-x^*)^2+12\zeta^2]}{[(x-x^*)^2+4\zeta^2]^2}\right\}dx^*, \tag{72}$$

where we have used the leading order pressure (31) to evaluate $p(x^*)=2x^*/(1+x^{*2})^2+\eta p^{(1)}$. We integrate (72) with respect to x^* to find

$$H\approx\frac{24\pi x(x^2-1)}{(1+x^2)^2}-\frac{4\pi x[x^4+2x^2(1+6\zeta+6\zeta^2)+(1+2\zeta)^2(1+8\zeta+24\zeta^2)]}{[x^2+(1+2\zeta)^2]^3}. \tag{73}$$

As in Sec. III, Eqs. (28) and (30) yield the system of equations to be solved for the pressure perturbation $p^{(1)}$:

$$\partial_x[6H+3(1+x^2)^2H+(1+x^2)^3\partial_x p^{(1)}]=0,\qquad p^{(1)}(-\infty)=p^{(1)}(\infty)=0. \tag{74}$$

Solving (73) and (74) yields

$$p^{(1)}=\frac{2\pi(2x^2-1)}{(1+x^2)^4}-\frac{\pi[12\zeta^2-20\zeta+30-x^2(45-60\zeta+36\zeta^2)+45x^4]}{2\zeta^4(1+x^2)^3}, \tag{75}$$

which we integrate with respect to x to find the dimensionless lift

$$L=\eta p^{(1)}dx=\eta C_i=\eta\frac{3\pi^2}{8}\left(1-\frac{30}{\zeta^4}\right)+O(\zeta^{-5}). \tag{76}$$

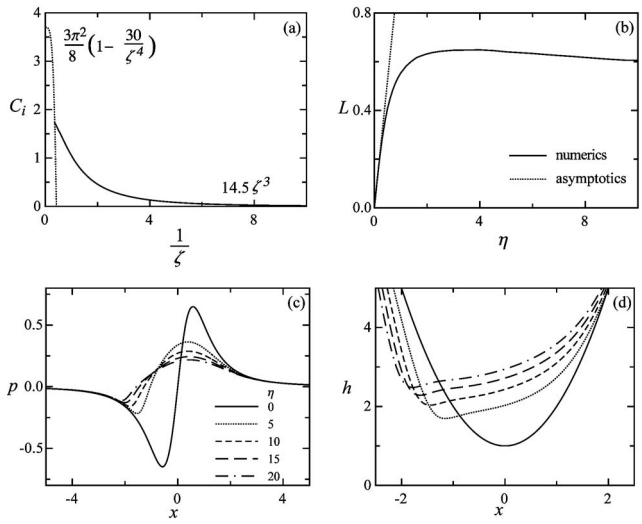

FIG. 12. For $\eta\ll 1$, $L=C_i(\zeta)\eta$ where $C_i(\zeta)$ is shown in (a). (b) shows the dimensionless lift per unit length L as a function of η for $\zeta=H_l/l_c=1$. (c) and (d) show pressure p and gap thickness h as a function of η. As the thickness of the layer decreases the presence of the undeformed substrate below is increasingly felt and the layer stiffens. In the linear regime a stiffer layer results in a smaller deformation and concomitant decrease in lift.

On the other hand, as $\zeta\to 0$ we approach the limit where the contact length is much larger than the layer thickness leading to the geometric stiffening. Due to solid incompressibility the layer may only deform via shear and the dominant term of the strain is $\nabla\mathbf{u}\sim u_x/H_l$. Since $\nabla\cdot\mathbf{u}=0$, we see that $u_x/l_c\sim H/H_l\to u_x/H_l\sim l_cH/H_l^2$. Balancing the strain energy per unit length $\int G(\nabla u)^2dA\sim G(l_cH/H_l^2)^2H_ll_c$ with the work done by the pressure p_0Hl_c yields $H\sim p_0H_l^3/Gl_c^2$ so that $\eta_{\zeta\to\infty}\sim p_0H_l^3/Gl_c^2h_0$. For a thin incompressible layer, the characteristic deflection is reduced by an amount $\eta_{\zeta\to\infty}/\eta\sim\zeta^{-3}$ so that $\lim_{\zeta\to\infty}C_i(\zeta)\sim\zeta^3$. C_i is displayed in Fig. 12(a). For intermediate values of ζ, we computed the results numerically.

The nonlinear problem arising for $\eta=O(1)$ is solved using (9), (10), (67), and (68). We first guess an initial gap profile h_{old}, then a shooting algorithm is employed to calculate the pressure distribution. The new pressure distribution is then used in (67) and (68) to calculate a new gap profile h_{new}. If $\int_{-10}^{10}(h_{\text{old}}-h_{\text{new}})^2dx<10^{-5}$ then the calculation is stopped, else we iterate with $h_{\text{old}}=h_{\text{new}}$. For $\zeta=1$, the results are shown in Figs. 12(b)–12(d). Not surprisingly, we find the same qualitative features discussed previously: L has a

maximum due to the competing effects of an increase in the gap thickness and the increased asymmetry of the contact zone.

VII. POROELASTIC LAYER

Motivated in part by the applications to the mechanics of cartilaginous joints, we now turn to the case of a cylinder moving above a fluid filled gel layer. This entails a different model for the constitutive behavior of the gel accounting for both the deformation of an elastic network and the concomitant fluid transport. To describe the mechanical properties of a fluid filled gel we use poroelasticity, the continuum description of a material composed of an elastic solid skeleton and an interstitial fluid.[27,35,36] Our choice of poroelasticity to model the gel is motivated by the following scaling argument.[37] Let $\boldsymbol{\nabla}$ and $\boldsymbol{\nabla}_{l_p}$ denote gradients on the system scale and the pore scale respectively; p_g is the pressure varying on the system scale due to the boundary conditions driving the flow, while p_p is the pressure varying on the microscopic scale due to pore geometry. Fluid stress balance on the pore scale implies that the sum of the macroscopic pressure gradient driving the flow, $\boldsymbol{\nabla} p_g$, and the microscopic pressure gradient $\boldsymbol{\nabla}_{l_p} p_p$ is balanced by the viscous resistance of the fluid having viscosity μ and velocity $\mathbf{v}$, $\mu \nabla_{l_p}^2 \mathbf{v}$, so that the momentum balance in the fluid yields

$$\mu \nabla_{l_p}^2 \mathbf{v} - \boldsymbol{\nabla} p_g - \boldsymbol{\nabla}_{l_p} p_p = 0. \tag{77}$$

When the pore scale l_p and system size H_l are well separated, i.e., $l_p/H_l \ll 1$, Eq. (77) yields the following scaling relations:

$$p_g \sim \frac{H_l \mu V}{l_p^2} \gg \frac{\mu V}{l_p} \sim p_p \tag{78}$$

from which we conclude that the dominant contribution to the fluid stress tensor comes from the pressure. The simplest stress-strain law for the composite medium, proposed by Biot,[27] is found by considering the linear superposition of the dominant components of the fluid and the solid-stress tensors. If strains are small, the elastic behavior of the solid skeleton is well characterized by isotropic Hookean elasticity. For a poroelastic material composed of a solid skeleton with Lamé coefficients G and λ when drained and a fluid volume fraction α, the stress tensor $\boldsymbol{\sigma}$ is given by the constitutive equation

$$\boldsymbol{\sigma} = G(\boldsymbol{\nabla}\mathbf{u} + \boldsymbol{\nabla}\mathbf{u}^{\mathrm{T}}) + \lambda \boldsymbol{\nabla} \cdot \mathbf{u}\mathrm{I} - \alpha p_g \mathrm{I}. \tag{79}$$

The equations of equilibrium are

$$\boldsymbol{\nabla} \cdot \boldsymbol{\sigma} = 0, \tag{80}$$

where we have neglected inertial effects. Mass conservation requires that the rate of dilatation of a solid skeleton having a bulk modulus β^{-1} is balanced by the entering fluid:

$$\frac{k}{\mu} \nabla^2 p_g = \beta \partial_t p_g + \partial_t \boldsymbol{\nabla} \cdot \mathbf{u}. \tag{81}$$

Here $\beta \neq \lambda + 2G/3$, since the Lamé coefficients λ and G are for the composite material and take into account the microstructure, while β^{-1} is independent of the microstructure; for cartilage $\beta^{-1} \sim 1$ GPa, while $G \sim \lambda \sim 1$ MPa. Equations (79)–(81) subject to appropriate boundary conditions describe the evolution of displacements $\mathbf{u}$ and fluid pressure p_g in a poroelastic medium.

We now calculate the response of a poroelastic gel to an arbitrary time-dependent pressure distribution before considering the specific case at hand. To make the equations dimensionless, we use the following scalings:

$$\begin{aligned} &x = \sqrt{2h_0 R}\, x', \quad z = H_l z', \quad t = \pi' = \frac{\sqrt{2h_0 R}}{V - \omega R} t', \\ &u_z = h_0 u_z', \quad u_x = h_0 u_x', \\ &p_g = p_0 p_g' = \mu(V - \omega R)\sqrt{\frac{2R}{h_0^3}}\, p_g', \quad p = p_0 p', \\ &\boldsymbol{\sigma} = p_0 \boldsymbol{\sigma}' = \mu(V - \omega R)\sqrt{\frac{2R}{h_0^3}}\, \boldsymbol{\sigma}'. \end{aligned} \tag{82}$$

We take the thickness of the layer to be much smaller than the length scale of the contact zone, $\zeta = H_l/\sqrt{2h_0 R} \ll 1$, and consider a compressible material, $G \sim \lambda$. Then after dropping primes, the stress tensor (79) becomes

$$\boldsymbol{\sigma} = \begin{pmatrix} \frac{1}{\eta}\frac{\lambda}{2G+\lambda}\partial_z u_z + \frac{\zeta}{\eta}\partial_x u_x - \alpha p_g & \frac{1}{\eta}\frac{G}{2G+\lambda}\partial_z u_x + \frac{\zeta}{\eta}\frac{G}{2G+\lambda}\partial_x u_z \\ \frac{1}{\eta}\frac{G}{2G+\lambda}\partial_z u_x + \frac{\zeta}{\eta}\frac{G}{2G+\lambda}\partial_x u_z & \frac{1}{\eta}\partial_z u_z + \frac{\zeta}{\eta}\frac{\lambda}{2G+\lambda}\partial_x u_x - \alpha p_g \end{pmatrix}. \tag{83}$$

Here,

$$\eta = \frac{p_0}{2G+\lambda}\frac{H_l}{h_0} = \sqrt{2}\frac{\mu(V-\omega R)}{2G+\lambda}\frac{H_l R^{1/2}}{h_0^{5/2}} \tag{84}$$

is the dimensionless number governing the relative size of the surface deflection to the undeformed gap thickness, i.e., the material compliance. Stress balance (80) yields

$$\begin{aligned} 0 &= \partial_{zz}u_x + \zeta\left(\frac{G+\lambda}{G}\partial_{xz}u_z - \eta\alpha\frac{2G+\lambda}{G}\partial_x p_g\right) \\ &\quad + \zeta^2\frac{2G+\lambda}{G}\partial_{xx}u_x, \\ 0 &= \partial_{zz}u_z - \eta\alpha\partial_z p_g + \zeta\frac{G+\lambda}{2G+\lambda}\partial_{xz}u_x + \zeta^2\frac{G}{2G+\lambda}\partial_{xx}u_z, \end{aligned} \tag{85}$$

and continuity (81) yields

$$\frac{k\tau}{\mu H_l^2\beta}(\partial_{zz}p_g + \zeta^2\partial_{xx}p_g) = \partial_t p_g + \frac{h_0}{\beta H_l p_0}\partial_t(\partial_z u_z + \zeta\partial_x u_x). \tag{86}$$

To leading order (85) and (86) reduce to

$$\begin{aligned} &\partial_{zz}u_x = 0, \\ &\partial_{zz}u_z - \alpha\eta\partial_z p_g = 0, \end{aligned} \tag{87}$$

and

$$\frac{k\tau}{\mu H_l^2\beta}\partial_{zz}p_g = \partial_t p_g + \frac{h_0}{\beta H_l p_0}\partial_{tz}u_z. \tag{88}$$

The normal unit vector to the soft interface is $\mathbf{n} = (-\partial_x u_z|_{z=0}, 1)$, which in dimensionless form is

$$\mathbf{n} = (-\varepsilon\partial_x u_z|_{z=0}, 1), \tag{89}$$

where $\varepsilon = \sqrt{h_0/2R}$. The balance of normal traction on the solid-fluid interface yields

$$\boldsymbol{\sigma}_f\cdot\mathbf{n}|_{z=0} = \boldsymbol{\sigma}_s\cdot\mathbf{n}|_{z=0}, \tag{90}$$

so that

$$\begin{aligned} &\partial_z u_x|_{z=0} = 0, \\ &\partial_z u_z|_{z=0} - \alpha\eta p_g|_{z=0} = -\eta p. \end{aligned} \tag{91}$$

At the interface between the soft film and the underlying rigid substrate the no-slip condition yields

$$u_z(x,-1) = 0, \quad u_x(x,-1) = 0. \tag{92}$$

Solving (87), (91), and (92) yields

$$\begin{aligned} &u_x = 0, \\ &-\eta p = -\alpha\eta p_g + \partial_z u_z. \end{aligned} \tag{93}$$

To calculate the displacement at the surface $u_z(x,0,t)$, we need to determine the fluid pressure in the gel p_g. Using (93) in (88) yields

$$\partial_t p_g - \gamma\partial_{zz}p_g = \delta\partial_t p, \tag{94}$$

where

$$\begin{aligned} \gamma &= \frac{\tau}{\tau_p} = \frac{k\sqrt{2Rh_0}(2G+\lambda)}{H_l^2(V-\omega R)[\beta(2G+\lambda)+\alpha]}, \\ \delta &= \frac{1}{\beta(2G+\lambda)+\alpha} \sim O(1). \end{aligned} \tag{95}$$

Here $\tau = l_c/V \sim \sqrt{h_0 R}/V$ is the time scale associated with motion over the contact length, $\tau_p \sim \mu H_l^2/kG$ is the time scale associated with stress relaxation via fluid flow across the thickness of the gel, and $\delta \sim 1/\alpha$ the inverse of the fluid volume fraction. Equation (94) corresponds to the short time limit discussed in Ref. 38. The boundary conditions for (94) are determined by the fact that at the solid-gel interface there is no fluid flux and at the fluid-gel boundary there is no pressure jump so that

$$\partial_z p_g(x,-1,t) = 0, \quad p_g(x,0,t) = p, \tag{96}$$

where both conditions are a consequence of Darcy's law for flow through a porous medium.

Although there is flux through the gel-fluid interface, the Reynolds equation (9) for the fluid pressure will remain valid if the fluid flux through the gel is much less than the flux through the thin gap. A fluid of viscosity μ flows with a velocity $\mathbf{v} = (v_x, v_z)$ through a porous medium of isotropic permeability k according to Darcy's law, so that $\mathbf{v} \sim k/\mu\boldsymbol{\nabla}p$. Hence, the total flux through a porous medium of thickness H_l is $\int_{-H_l}^{0} v_x dz$, which will scale as $H_l k p_0/\mu\sqrt{h_0 R} \sim H_l k V/\mu h_0^2$. Comparing this with the flux through the thin gap $h_0 V$ leads to the dimensionless group $Q_R = H_l k/h_0^3$. If $Q_R \ll 1$, we can neglect the flow through the porous medium. For cartilage, $H_l \sim 1$ mm and $k \sim 10^{-14}$ mm^2, and flow through the porous medium can be neglected if $h_0 \gg 10$ nm. This implies that the Reynolds lubrication approximation embodied in (9) remains valid in the gap for situations of biological interest.

In response to forcing, a poroelastic material can behave in three different ways depending on the relative magnitude of the time scale of the motion $\tau = l_c/V$ and the poroelastic time scale τ_p. If $\tau \gg \tau_p$, the fluid in the gel is always in equilibrium with the surrounding fluid and a purely elastic theory for the deformation of the gel suffices; if $\tau \sim \tau_p$, the gel will behave as a material with a "memory;" if $\tau \ll \tau_p$, the fluid has no time to move relative to the matrix and the poroelastic material will again behave as a solid albeit with a higher elastic modulus. In the physiological case of a cartilage layer in a rotational joint, the poroelastic time scale for bovine articular cartilage is reported to be between $\tau_p \approx 20$ s (Ref. 7) and $\tau_p \approx 500$ s.[9] For time scales on the order of 1 s, the cartilage should behave as a solid but with an elastic modulus greater than that measured by equilibrium studies. We consider three different cases which are as follows.

A. Low speed: $\tau_m \gg \tau_p$

When the cylinder moves slowly, $\tau_m \gg \tau_p$, the time scale of the motion is much larger than the time scale over which the pressure diffuses (i.e., $\gamma \gg 1 \sim \delta$) so that (94) becomes

$$\partial_{zz} p_g = 0. \tag{97}$$

Solving (97) subject to (96) yields

$$p_g = p, \tag{98}$$

i.e., at low speeds the fluid pressure in the gel is the same as the fluid pressure outside the gel. Equations (92) and (93) can be solved to yield

$$u_z(x,0,t) = -(1-\alpha)\eta p(x,t). \tag{99}$$

We see that this limit gives a local relationship between the displacement of the gel surface and the fluid pressure in the gap, exactly as in the case of a purely elastic layer treated in Sec. III.

B. High speed: $\tau_m \ll \tau_p$

When the time scale of the motion is much smaller than the time scale over which the pressure diffuses, i.e., $\gamma \ll 1 \sim \delta$, (94) becomes

$$\partial_t p_g = \delta \partial_t p. \tag{100}$$

Since the gel is at equilibrium with the external fluid before the cylinder passes over it, $p_g(x,z,-\infty) = p(x,-\infty) = 0$, and Eq. (100) yields

$$p_g(x,z,t) = \delta p(x,t). \tag{101}$$

Inserting (101) into (93) and integrating yields

$$u_z(x,0,t) = \frac{-\beta(2G+\lambda)\eta}{\beta(2G+\lambda)+\alpha} p(x,1,t). \tag{102}$$

In this limit, the fluid has no time to flow through the pores and the only compression is due to bulk compressibility of the composite gel, which now behaves much more rigidly. The effective elastic modulus of the solid layer is now $G_{\text{eff}} \sim \beta^{-1} \sim 1$ GPa rather than $G_{\text{eff}} \sim 1$ MPa. However, the relationship between the pressure and the displacement remains local as in Sec. III.

We note that if $\nabla \cdot \mathbf{u} = 0$, (81) has no forcing term and $p_g = 0$. Poroelastic theory does not take into account shear deformations since these involve no local change in fluid volume fraction in the gel. In this case, all the load will be borne by the elastic skeleton. However, shear deformation in a thin layer will involve geometric stiffening due to incompressibility so that the effective modulus will be $G_{\text{eff}} \sim (h_0 R/H_l^2) G$.[30] Hence, if $(h_0 R/H_l^2) G\beta \ll 1$, the deformation should be treated as an incompressible layer as in Sec. VI. If $(h_0 R/H_l^2) G\beta \gg 1$, the layer should be treated as in Sec. III with an effective modulus β^{-1}.

C. Intermediate speeds: $\tau_m \sim \tau_p$

When $\delta \sim \gamma \sim 1$, rewriting (94) for the difference between the fluid pressure inside and outside the gel, $p_g(x,z,t) - p(x,t)$, yields

$$\partial_t (p_g - p) - \gamma \partial_{zz} (p_g - p) = (\delta - 1)\partial_t p, \tag{103}$$

with the boundary conditions

$$\partial_z (p_g - p)(x,-1,t) = 0, \quad (p_g - p)(x,0,t) = 0. \tag{104}$$

We expand $p_g - p$ in terms of the solution of the homogeneous part of (103) and (104):

$$p_g - p = \sum_{n=0}^{\infty} A_n(t) \sin \pi\left(n + \tfrac{1}{2}\right) z. \tag{105}$$

Inserting the expansion into (103), we find

$$\sum_{n=0} \left[\partial_t A_n + \gamma \pi^2 \left(n + \tfrac{1}{2}\right)^2 A_n\right] \sin \pi\left(n + \tfrac{1}{2}\right) z = (\delta - 1)\partial_t p. \tag{106}$$

Multiplying (106) with $\sin \pi\left(m + \frac{1}{2}\right) z$ and integrating over the thickness yields

$$\partial_t A_n + \gamma \pi^2 \left(n + \frac{1}{2}\right)^2 A_n = \frac{2(1-\delta)}{\pi\left(n + \frac{1}{2}\right)} \partial_t p. \tag{107}$$

Solving (107) for $A_n(t)$ yields

$$A_n(t) = \frac{2(1-\delta)}{\pi\left(n + \frac{1}{2}\right)} \int_{-\infty}^{t} e^{-\gamma \pi^2 (n+1/2)^2 (t-t')} \partial_{t'} p \, dt'. \tag{108}$$

Substituting (108) into (105) yields the fluid pressure in the gel,

$$p_g = p + \sum_{n=0} \frac{2(1-\delta) \sin \pi\left(n + \frac{1}{2}\right) z}{\pi\left(n + \frac{1}{2}\right)} \times \int_{-\infty}^{t} e^{-\gamma \pi^2 (n+1/2)^2 (t-t')} \partial_{t'} p \, dt'. \tag{109}$$

Finally, (92), (93), and (109) yield

$$u_z(1) = \eta \left[(-1+\alpha) p + \alpha \sum_{n=0} \frac{2(\delta - 1)}{\pi^2 \left(n + \frac{1}{2}\right)^2} \int_{-\infty}^{t} e^{-\gamma \pi^2 (n+1/2)^2 (t-t')} \partial_{t'} p \, dt' \right]. \tag{110}$$

Since the higher order diffusive modes ($n > 0$) decay more rapidly than the leading order diffusive mode ($n = 0$), a good approximation to (110) is

$$-\eta H(x) = u_z(0) = \eta \left[(-1+\alpha) p + \alpha \frac{8(\delta - 1)}{\pi^2} \int_{-\infty}^{t} e^{(-\gamma \pi^2/4)(t-t')} \partial_{t'} p \, dt' \right]. \tag{111}$$

This approximation is similar to that used in Ref. 37. To simplify (111) for the case of interest, we define

$$\xi = \int_{-\infty}^{t} e^{(-\gamma\pi^2/4)(t-t')} \partial_{t'} p \, dt', \tag{112}$$

so that

$$\partial_t \xi = -\frac{\gamma\pi^2}{4}\xi + \partial_t p. \tag{113}$$

In the reference frame of the steadily moving cylinder $\xi(x,t)=\xi(x-t)$, so that

$$\partial_x \xi = \frac{\gamma\pi^2}{4}\xi + \partial_x p. \tag{114}$$

Integrating the above yields

$$\xi = -\int_{x}^{\infty} e^{(-\gamma\pi^2/4)(x'-x)} \partial_{x'} p \, dx'. \tag{115}$$

Consequently, the distance between the gel and the cylinder is found from (11), (111), (112), and (115) to be

$$h(x) = 1 + x^2 + \eta(1-\alpha) \times \left[p + \frac{8}{\pi^2}\int_{x}^{\infty} e^{(-\gamma\pi^2/4)(x'-x)} \partial_{x'} p \, dx' \right], \tag{116}$$

where

$$\eta = \frac{p_0 H_l}{(2G+\lambda)h_0} = \frac{\sqrt{2R}H_l \mu (V-\omega R)}{h_0^{5/2}(2G+\lambda)}, \tag{117}$$

where we are considering the case in which the bulk modulus of the skeletal material is much larger than the modulus of the elastic matrix $\beta G \ll 1$, so that (95) implies $\delta \approx 1/\alpha$. This leaves us a system of equations (9), (10), and (116) for the pressure with two parameters: η characterizes the deformation (softness) and γ is the ratio of translational to diffusive timescales. The two limits $\gamma \ll 1$ and $\gamma \gg 1$ of (116) can both be treated using asymptotic methods. For $\gamma \gg 1$, (116) yields

$$h = 1 + x^2 + \eta(1-\alpha)p, \tag{118}$$

and we recover the limit of a thin compressible elastic layer treated in Sec. III with $\eta \to (1-\alpha)\eta$. For $\gamma \ll 1$, (116) yields

$$h = 1 + x^2 + \left(1 - \frac{8}{\pi^2}\right)(1-\alpha)\eta p, \tag{119}$$

which is the result for a thin compressible layer with $\eta \to (1-8/\pi^2)(1-\alpha)\eta$. When $\eta \ll \gamma \ll 1$, we expand the pressure field as in (26) writing $p = p_0 + \eta p_1$, where $p_0 = 2x/(1+x^2)^2$ as in (31). Inserting this expression into (116) yields

$$h = 1 + x^2 + \eta(1-\alpha)\left\{ p_0 + \frac{8}{\pi^2} \times \int_{x}^{\infty} \left[1 + \frac{\pi^2\gamma}{4}(x-x') \right] \partial_{x'} p_0 dx' \right\} + O(\gamma\eta), \tag{120}$$

which can be integrated to give

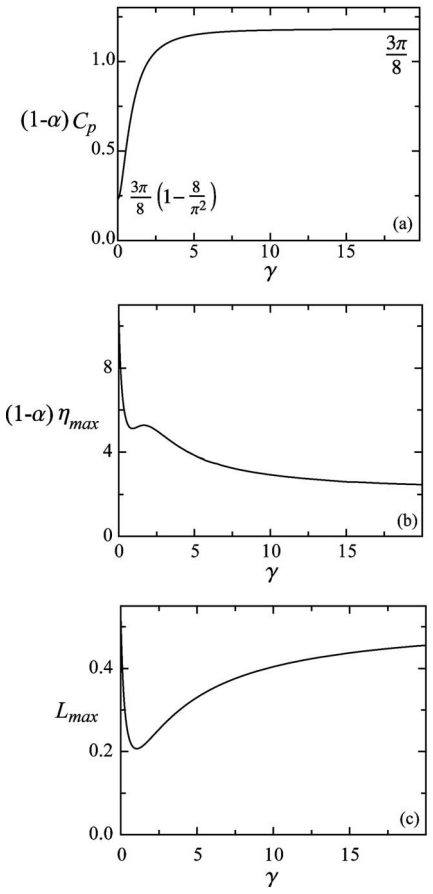

FIG. 13. For $\eta \ll 1$, $L = C_p(\gamma)\eta$ where γ is the ratio of translational to poroelastic time scales, and $C_p(\gamma)$ is shown in (a). (b) $\eta_{\max}$, the value of η at which the lift is maximum, plotted against γ. (c) The maximum lift $L_{\max}$ as a function of γ. After scaling L and η, $L[\eta/\eta_{\max}(\gamma)]/L_{\max}(\gamma)$, the curves can be almost perfectly collapsed onto a single curve.

$$h = 1 + x^2 + \eta(1-\alpha)\left[\frac{(\pi^2-8)2x}{\pi^2(1+x^2)^2} + \frac{2\gamma}{(1+x^2)} \right]. \tag{121}$$

We see that increasing γ increases the gap thickness and lowers the pressure without increasing the asymmetry, thus decreasing the lift. In the small deflection limit, $\eta \ll 1$, the dimensionless lift force is $L = C_p(\gamma)\eta$ and the lift force in dimensional terms is

$$L = C_p(\gamma)(1-\alpha)\frac{\mu^2 V^2}{2G+\lambda}\frac{H_l R^{3/2}}{h_0^{7/2}}, \tag{122}$$

where C_p is a function of γ and shown graphically in Fig. 13(a).

When $\eta = O(1)$, we use a numerical method to solve (9), (10), and (116) on a finite domain using the continuation software AUTO2000 (Ref. 31) with η and γ as the continuation parameters. The initial solution from which the continuation begins is with $\eta = \gamma = 0$, corresponding to $h = 1 + x^2$, and $p = 2x/(1+x^2)^2$. The form of the lift force as a function of η, $L(\eta,\gamma)$ for various γ can be almost perfectly collapsed onto a single curve after appropriately scaling the η, L axes using the position of the maximum, i.e., $L[\eta/\eta_{\max}(\gamma)]/L_{\max}(\gamma)$ where $L_{\max}$ and $\eta_{\max}$ are shown in Figs. 13(b) and 13(c).

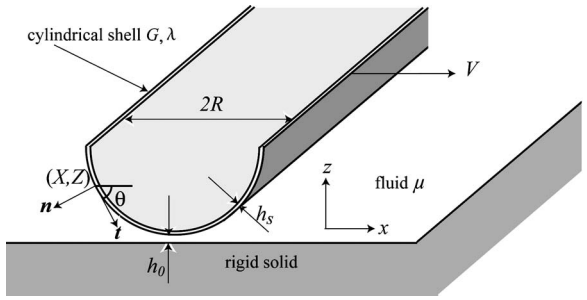

FIG. 14. Schematic diagram of a half cylinder of radius R, thickness h_s, and Lamé coefficients μ and λ moving at a velocity V while completely immersed in a fluid of viscosity μ. The edges of the half cylinder are clamped at a distance $R+h_0$ from the surface of an undeformed solid. θ denotes the angle between the tangent to the surface and the x axis. $[X(s),Z(s)]$ are the laboratory frame coordinates of the half cylinder as a function of the arc-length coordinate s.

VIII. ELASTIC SHELL

For elastic layers attached to a rigid substrate the effective stiffness increases with decreasing thickness. However, for free elastic shells the effective stiffness increases with increasing thickness. To see the effects of this type of geometry in biolubrication problems, we turn our attention to a configuration in which a surface is rendered soft through its geometry rather than its elastic moduli. We consider a half-cylindrical elastic shell of thickness h_s and radius R moving with constant velocity V parallel to the rigid substrate, while completely immersed in fluid of viscosity μ, as shown in Fig. 14. The shell is clamped at its edges, which are at a height $R+h_0$ above the rigid solid. The shape of the elastic half cylinder is governed by the *elastica* equation (for the history of the elastica equation as well as its derivation see Ref. 39) for $\theta(s)$, the angle between the horizontal and the tangent vectors where s is the arc-length coordinate. Balancing torques about the point O in Fig. 15 gives: $M(s+ds)-M(s)-ds n_x \sin\theta + ds n_z \cos\theta + ds^2/2(p\cos\theta - \mu\partial_z u \sin\theta - p\partial_s h \sin\theta)=0$. In the limit $ds\to 0$, $\partial_x M - n_x \sin\theta + n_z \cos\theta = 0$. The x-force balance is $n_x(s+ds) - n_x(s) - ds(p\partial_s h + \mu\partial_x u)=0$, which as $ds\to 0$ yields $\partial_s n_x = \mu\partial_x u + p\partial_s h$. The z-force balance is $n_z(s+ds) - n_z(s) + p\,ds = 0$, which as $ds\to 0$ yields $\partial_s n_z = -p$. We note that external forces are applied in the contact region where derivatives taken with respect to x are interchangeable with those taken with respect to s, i.e., $\partial_x h \approx \partial_s h$ and $\partial_x p \approx \partial_s p$, which allows for a consistent framework for the fluid and the solid equilibrium equations. This yields

$$\frac{G(\lambda+G)h_s^3}{3(\lambda+2\mu)}\partial_{ss}\theta = n_x \sin\theta - n_z\cos\theta, \tag{123}$$

where the stress resultants n_x and n_z are determined by the equations

$$0=\partial_s n_x + \mathbf{e_x}\cdot\boldsymbol{\sigma}_f\cdot\mathbf{n}, \quad 0=\partial_s n_z + \mathbf{e_z}\cdot\boldsymbol{\sigma}_f\cdot\mathbf{n}, \tag{124}$$

i.e.,

$$\partial_s n_x = \frac{\mu V}{h} + \frac{h\partial_s p}{2} + p\partial_s h, \quad \partial_s n_z = -p, \tag{125}$$

where $\mathbf{n}=(\partial_s h,-1)$, and $\boldsymbol{\sigma}_f$ is given by (2). Then, the pressure in the fluid is governed by the Reynolds equation (9),

$$\partial_{ss} p = \frac{-\partial_s h}{h^3}(6\mu V + 3h^2\partial_s p). \tag{126}$$

Finally, since cylindrical deformations are inextensional, we must complement (123)–(126) with the kinematic equations

$$\partial_s X = \cos\theta, \quad \partial_s h = \sin\theta, \tag{127}$$

where the position of the surface of the elastic cylinder is (X,h). Equations (123)–(127) are made dimensionless with the following scalings:

$$p = p_0 p' = \frac{\sqrt{2}\mu V R^{1/2}}{h_0^{3/2}}p', \quad s=\pi R s', \quad h = RZ,$$
$$X = RX', \quad n_x = p_0 h_0 n_x', \quad n_z = p_0\sqrt{2h_0 R}\,n_z'. \tag{128}$$

After dropping primes, the dimensionless forms of Eqs. (123)–(127) are written as

$$\partial_{ss} p = \frac{-\partial_s Z}{Z^3}\left[3\sqrt{2}\pi\left(\frac{h_0}{R}\right)^{3/2} + 3Z^2\partial_s p\right], \tag{129}$$

$$\partial_s n_x = \frac{R}{h_0}\left(p\partial_s Z + \frac{Z\partial_s p}{2}\right) + \sqrt{\frac{h_0}{2R}}\frac{\pi}{Z}, \tag{130}$$

$$\partial_s n_z = -\pi\sqrt{\frac{R}{2h_0}}p, \tag{131}$$

$$\partial_s X = \pi\cos\theta, \tag{132}$$

$$\partial_s Z = \pi\sin\theta, \tag{133}$$

$$\partial_{ss}\theta = 3\sqrt{2}\pi^2\frac{\mu V(\lambda+2G)}{G(\lambda+G)} \times \frac{R^{5/2}}{h_s^3 h_o^{1/2}}\left(n_x\sin\theta - \sqrt{\frac{2R}{h_0}}n_z\cos\theta\right). \tag{134}$$

To find the scale of the elastic deformation $\eta=H_0/h_0$, where the maximum displacement of the cylinder is of order H_0, we note that the change in curvature is of order H_0/R^2 so that the bending strain is $\epsilon=h_s H_0/R^2$ and the elastic energy per

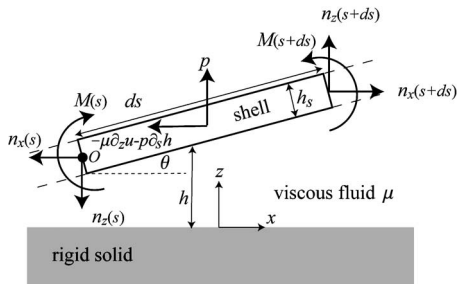

FIG. 15. Schematic of the torque and the force balance for a bent cylindrical shell of thickness h_s and Lamé coefficients G and λ subject to a traction $(-\mu\partial_z u - p\partial_s h, p)$ applied by a viscous fluid. x and z are coordinates in the reference frame of the rigid solid, while s is the arc-length coordinate in the shell. $M(s)=[G(\lambda+G)h_s^3/3(\lambda+2G)]\partial_{ss}\theta$ is the bending moment.

unit length, therefore, scales as $\int G\epsilon^2 dA \sim \int G(h_s H_0/R^2)^2 dA \sim G h_s^3 H_0^2/R^3$. The work done by the fluid is due to a localized torque and scales as $\int pxdx \sim p_0 h_0 R$, acting through an angle $\Delta\theta \sim H_0/R$. Balancing the work done by the fluid torque $p_0 h_0 H_0$ with the elastic energy $G h_s^3 H_0^2/R^3$ yields

$$\eta \sim \frac{H_0}{h_0} \sim \frac{\mu V}{G}\frac{R^{7/2}}{h_s^3 h_0^{3/2}}, \tag{135}$$

so that (134) can be written as

$$\partial_{ss}\theta = \frac{h_0\eta}{R}\left(n_x \sin\theta - \sqrt{\frac{2R}{h_0}} n_z \cos\theta\right). \tag{136}$$

The system (129)–(133) and (136) for θ, p, n_x, n_z, x, and z has two dimensionless parameters, $\eta = 3\sqrt{2}\pi^2[\mu V(\lambda + 2G)/G(\lambda+G)]R^{7/2}/h_s^3 h_0^{3/2}$ and h_0/R, and is subject to eight boundary conditions

$$\begin{aligned} &p(0) = p(1) = 0, \\ &X(0) = -1, \quad X(1) = 1, \\ &Z(0) = Z(1) = 1 + \frac{h_0}{R}, \\ &\theta(0) = \frac{-\pi}{2}, \quad \theta(1) = \frac{\pi}{2}. \end{aligned} \tag{137}$$

The first two are a consequence of lubrication theory, while the rest are kinematic boundary conditions on the cylinder's lateral edges, which are assumed to be clamped. We note that if the cylinder has a natural curvature this will not affect the system of equations (123)–(127), but may change the boundary conditions.

We solve (129)–(133), (136), and (137) numerically using the continuation software AUTO2000 (Ref. 31) with η as the continuation parameter. For $\eta < 1$, the dimensionless lift $L = C_s\eta$, where the constant $C_s(h_0/R)$ is shown in Fig. 17(b). However, we see that even for $\eta < 100$ the linear relationship remains valid. The dimensional lift force for $\eta < 100$ is

$$L = 6\sqrt{2}\pi^2 \frac{\mu^2 V^2(\lambda + 2G)}{G(\lambda+G)}\frac{R^{9/2}}{h_s^3 h_0^{5/2}} C_s\left(\frac{h_0}{R}\right). \tag{138}$$

Figures 16 and 17(a) show the gap thickness profile and pressure distribution for $h_0/R = 0.001$. As η increases the elastic deformation breaks the symmetry of the gap thickness profile and results in an asymmetric pressure distribution and corresponding lift. However, the concomitant increase in gap thickness decreases the magnitude of the pressure. As for the previous systems considered, the competition between symmetry breaking (dominant for small η) and decreasing pressure (dominant for large η) produces a maximum in the lift. The form of the lift force as a function of η, $L(\eta, h_0/R)$ for various h_0/R can be almost perfectly collapsed onto a single curve after appropriately scaling the η, L axes; i.e., $L[\eta/\eta_{\max}(h_0/R)]/L_{\max}(h_0/R)$ where $L_{\max}$ and $\eta_{\max}$ are shown in Figs. 17(c) and 17(d).

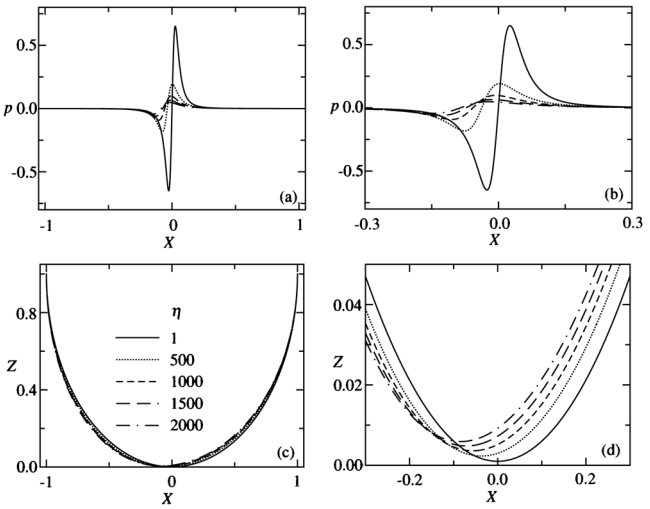

FIG. 16. (a) and (b) pressure distribution $p(X)$ as a function of the softness, η. As η increases the asymmetry of the pressure distribution increases and the maximum pressure decreases. (c) and (d) shape of the sheet, where $X(s)$ and $Z(s)$ are the coordinates of the center line in the laboratory frame. We see that the point of nearest contact is pulled back and the symmetry of the profile is broken by the forces exerted by the fluid on the cylindrical shell. $h_0/R = 10^{-3}$.

IX. JOURNAL BEARING

So far, with the exception of Sec. IV, we have dealt only with nonconforming contacts. In this section, we consider an elastohydrodynamic journal bearing: a geometry consisting of a cylinder rotating within a larger cylinder that is coated with a soft solid. The journal bearing is a conforming contact and is a better representation of biolubrication in mammalian joints in which synovial fluid lubricates bone coated with thin soft cartilage layers. Previous analyses of the elastohydrodynamic journal bearing have focused on situations where fluid cavitation needs to be taken into account.[3,6] As

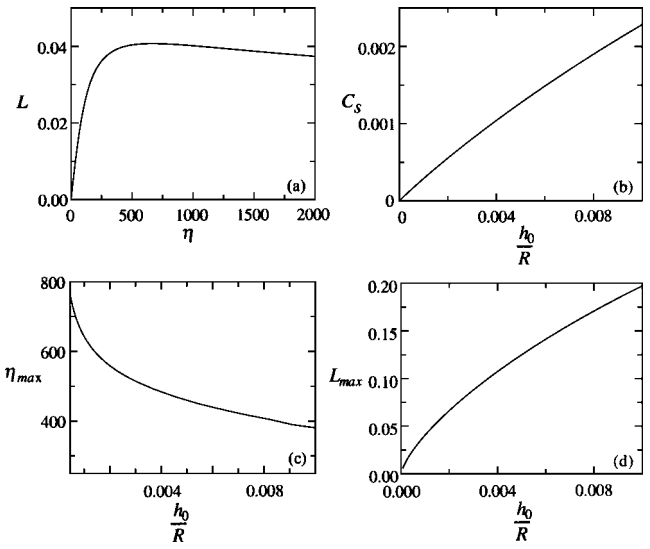

FIG. 17. (a) Dimensionless lift on a cylindrical shell with $h_0/R = 10^{-3}$. For $\eta < 100$. $L = C_s(h_0/R)\eta$, where C_s is shown in (b). The form of $L(\eta, h_0/R)$ can be almost perfectly collapsed onto a single curve after appropriately scaling the η, L axes, i.e., $L[\eta/\eta_{\max}(h_0/R)]/L_{\max}(h_0/R)$, where $\eta_{\max}$ and $L_{\max}$ are shown in (c) and (d) respectively.

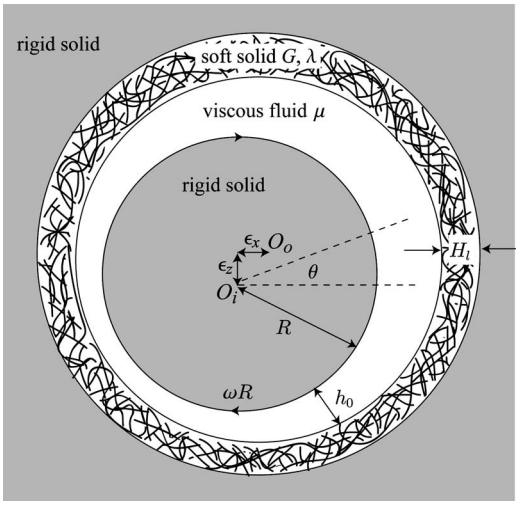

FIG. 18. Schematic diagram of the modified journal bearing geometry in which the larger cylinder of radius $R+H_l+h_0$ has been coated by a soft solid of thickness H_l having Lamé coefficients G and λ. The larger cylinder's axis is located a distance ϵ_x in the x direction and a distance ϵ_z in the z direction from the axis of the inner cylinder of radius R. The average gap thickness is h_0.

before, we restrict our attention in the case where the surface deforms appreciably before the cavitation threshold is reached so that the gap remains fully flooded. A schematic diagram is shown in Fig. 18.

We take the center of the inner cylinder, O_i, to be the origin; the center of the outer cylinder, O_o, is located at $x=\epsilon_x$, $z=\epsilon_z$. The inner cylinder of radius R rotates with angular velocity ω; the stationary outer cylinder of radius $R+h_0+H_l$ is coated with a soft solid of thickness $H_l \ll R$ and Lamé coefficients λ and G. Here, h_0 is the average distance between the inner cylinder and the soft solid. Following Leal,[28] we use cartesian coordinates to describe the eccentric geometry and applied forces, but use polar coordinates to describe the fluid motion. When $h_0/R \ll 1$, the lubrication approximation reduces the Stokes equations in a cylindrical geometry for a fluid of viscosity μ, pressure p, and velocity field $\mathbf{v}=(v_r, v_\theta)$ to[28]

$$\partial_r p = 0, \quad \frac{1}{R}\partial_\theta p = \mu \partial_{rr} v_\theta, \tag{139}$$

subject to the boundary conditions

$$\begin{aligned} &v_r = 0, \quad v_\theta = -\omega R \quad \text{at } r = R, \\ &v_r = 0, \quad v_\theta = 0 \quad \text{at } r = R + h, \\ &p(0) = p(2\pi). \end{aligned} \tag{140}$$

Since $h_0/R \ll 1$, the continuity equation simplifies to[28]

$$R\partial_r v_r + \partial_\theta v_\theta = 0, \tag{141}$$

and the gap thickness profile simplifies to

$$h(\theta) = h_0 + \epsilon_x \cos\theta + \epsilon_z \sin\theta + H(\theta), \tag{142}$$

where $H(\theta)$ is the elastic interface displacement due to the fluid forces. As in Sec. III,

$$H(\theta) = \frac{H_l p(\theta)}{2G+\lambda}, \tag{143}$$

so that (142) yields

$$h = h_0 + \epsilon_x \cos\theta + \epsilon_z \sin\theta + \frac{H_l p}{2G+\lambda}. \tag{144}$$

Using the following primed dimensionless variables:

$$\begin{aligned} &v_r = \omega h_0 v_r', \quad v_\theta = \omega R v_\theta', \quad r = h_0 r', \quad h = h_0 h', \\ &p = p^* p' = \frac{\mu R^2 \omega}{h_0^2} p', \quad \epsilon_x = h_0 \epsilon_x', \quad \epsilon_z = h_0 \epsilon_z', \end{aligned} \tag{145}$$

we write (139)–(141) and (144), after dropping the primes, as

$$\begin{aligned} &\partial_r p = 0, \\ &\partial_\theta p = \partial_{rr} v_\theta, \\ &\partial_r v_r + \partial_\theta v_\theta = 0, \\ &h = 1 + \epsilon_x \cos\theta + \epsilon_z \sin\theta + \eta p, \end{aligned} \tag{146}$$

subject to

$$\begin{aligned} &v_r = 0, \quad v_\theta = -1 \quad \text{at } r = \frac{R}{h_0}, \\ &v_r = 0, \quad v_\theta = 0 \quad \text{at } r = \frac{R}{h_0} + h, \\ &p(0) = p(2\pi), \end{aligned} \tag{147}$$

where

$$\eta = \frac{H_l p^*}{h_0(2G+\lambda)} = \frac{\mu\omega R^2 H_l}{(2G+\lambda)h_0^3} \tag{148}$$

is the softness parameter. As in Sec. II, we use (146) to derive the system of equations for the fluid pressure,

$$\begin{aligned} &\partial_\theta(6h + h^3 \partial_\theta p) = 0, \\ &h = 1 + \epsilon_x \cos\theta + \epsilon_z \sin\theta + \eta p, \\ &p(0) = p(2\pi). \end{aligned} \tag{149}$$

In addition, fluid incompressibility implies that the average deflection must vanish:

$$\int_0^{2\pi} h \, d\theta = 2\pi \rightarrow \int_0^{2\pi} p \, d\theta = 0. \tag{150}$$

The forces on the inner cylinder are

$$\int_0^{2\pi} p \sin\theta \, d\theta = L_z, \quad \int_0^{2\pi} p \cos\theta \, d\theta = L_x. \tag{151}$$

Here, L_z is the vertical force and L_x is the horizontal force. We begin with the classical solution for a rigid journal bearing:[28] $L_z=1$, $L_x=\eta=\epsilon_z=0$, $\epsilon_x=0.053$.

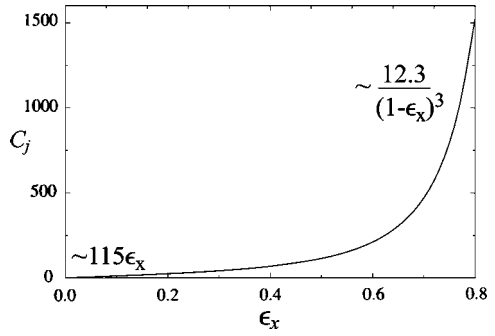

FIG. 19. For small η the dimensionless horizontal force, $L=C_j(\epsilon_x)\eta$, where the coefficient C_j is plotted above.

As in previous sections, we investigate how elastohydrodynamics alters this picture by specifying the eccentricity (ϵ_x, ϵ_z) and calculating the forces (L_x, L_z) as a function of the softness parameter η. Solutions to (149)–(151) are computed numerically using the continuation software AUTO2000 (Ref. 31) with η as the continuation parameter and the solution for $\eta=0$ as the initial guess. Just as for different geometries analyzed in previous sections, the deflection of the surface of the soft solid breaks the symmetry and leads to the generation of a horizontal force in the x direction: $L_x>0$. For small deformations ($\eta \ll 1$), the dimensionless horizontal force $L=C_j(\epsilon_x)\eta$, where the coefficient $C_j(\epsilon_x)$ is shown in Fig. 19. In dimensional terms, the horizontal force per unit length for small deformations is

$$L_x = C_j(\epsilon_x)\frac{p^* H_l}{(2G+\lambda)h_0} p^* R = C_j(\epsilon_x)\frac{\mu^2\omega^2 R^5 H_l}{(2G+\lambda)h_0^5}. \qquad (152)$$

For nearly concentric cylinders, $\epsilon_x \ll 1$, $C_j(\epsilon_x)=115\epsilon_x + O(\epsilon_x^2)$. For large eccentricities, $\epsilon_x \to 1$, the lubrication pressure diverges and $C_j(\epsilon_x) \approx 12.3(1-\epsilon_x)^{-3}$. For $\eta \ll 1$, we show L, h, and p in Fig. 20.

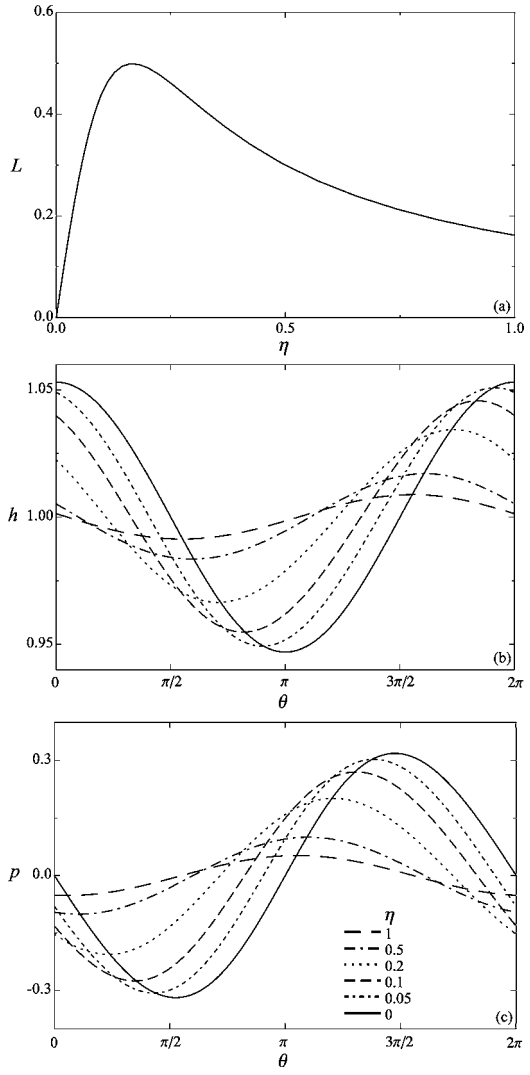

FIG. 20. (a) Dimensionless horizontal force L acting on the inner cylinder as a function of η, a measure of the surface deflection; (b) the corresponding gap thickness profiles; (c) the corresponding pressure profiles. $\epsilon_z=0$, $\epsilon_x=0.053$.

X. THREE-DIMENSIONAL LUBRICATION FLOW

The analysis of the three-dimensional problem of a sphere moving close to a soft substrate is considerably more involved. Here, we restrict ourselves to scaling arguments to generalize the quantitative results of previous sections to spherical sliders. The results are tabulated in Table II. In the fluid layer separating the solids, balancing the pressure gradient with the viscous stresses yields

$$\frac{p}{l_c} \sim \frac{\mu V}{h^2} \to p \sim \frac{\mu V l_c}{h^2}, \qquad (153)$$

where l_c is the size of the contact zone. Substituting $h=h_0+H_0$ with $H_0 \ll h_0$, we find that the lubrication pressure is

$$p \sim \frac{\mu V l_c}{(h_0+H_0)^2} \sim \frac{\mu V l_c}{h_0^2}\left(1+\frac{H_0}{h_0}\right) = \frac{\mu V l_c}{h_0^2}(1+\eta). \qquad (154)$$

The reversibility of Stokes equations and the symmetry of paraboloidal contacts implies that the lift force $L=0$ when $\eta=H_0/h_0=0$. For $\eta \ll 1$, we expand the pressure as $p=p^{(0)}+\eta p^{(1)}$. Since $p=p^{(0)}$ will not generate vertical forces, the lift on a spherical slider L_s will scale as

$$L_s = \eta \int p^{(1)} dA \sim \eta \int \frac{\mu V l_c}{h_0^2} dA \sim \eta \frac{\mu V l_c^3}{h_0^2}. \qquad (155)$$

To compute L, we need a prescription for the softness η and the contact radius l_c for each configuration.

(a) For a thin compressible elastic layer (Sec. III), we substitute $l_c \sim \sqrt{h_0 R}$ and $\eta \sim [\mu(V-\omega R)/2G+\lambda] \times (H_l R^{1/2}/h_0^{5/2})$ into (155) to find

$$L_s \sim \frac{\mu^2 V^2}{2G+\lambda}\frac{H_l R^2}{h_0^3}. \qquad (156)$$

(b) For a thin elastic layer with a degenerate axisymmetric conforming contact (Sec. IV), $l_c \sim (h_0 R^{2n-1})^{1/2n}$ and $\eta \sim (\mu V/2G+\lambda)(H_l R^{1-1/2n}/h_0^{3-1/2n})$ so that (155) yields

$$L_s \sim \frac{\mu^2 V^2}{2G+\lambda}\frac{H_l R^{4-(2/n)}}{h_0^{5-(2/n)}}. \qquad (157)$$

(c) For a soft spherical slider (or thick layer $H_l \gg l_c$; Sec. V), the deflection is given by (45) so that

$$H(x,y) = \frac{\lambda + 2G}{4\pi G(\lambda + G)} \int \frac{p(x',y')dx'dy'}{\sqrt{(x'-x)^2 + (y'-y)^2}} \sim \frac{pl_c}{G}, \tag{158}$$

so that

$$\eta \sim \frac{pl_c}{Gh_0}, \tag{159}$$

the size of the contact zone is $l_c \sim \sqrt{h_0 R}$, so that (155) and (159) yield

$$L_s \sim \frac{\mu^2 V^2}{G} \frac{R^{5/2}}{h_0^{5/2}}. \tag{160}$$

(d) For an incompressible layer (Sec. VI), we have two cases depending on the thickness of the substrate relative to the contact zone characterized by the parameter $\zeta = H_l/l_c$. For $\zeta \gtrsim 1$, $l_c \sim \sqrt{h_0 R}$ and $\eta \sim [\mu(V-\omega R)/G](R/h_0^2)$ so that (155) yields

$$L_{\zeta \gtrsim 1} \sim \frac{\mu^2 V^2}{G} \frac{R^{5/2}}{h_0^{5/2}}. \tag{161}$$

For the case $\zeta \ll 1$, the proximity of the undeformed substrate substantially stiffens the layer. In sharp contrast to a compressible layer, a thin incompressible layer will deform via shear with an effective shear strain $\Delta u/H_l$. An incompressible solid must satisfy the continuity equation, $\nabla \cdot \mathbf{u} = 0$, which implies that $\Delta u/l_c \sim H_0/H_l$. Consequently, $\Delta u/H_l \sim l_c H_0/H_l^2$. Balancing the elastic energy $\int G(l_c H_0/H_l^2)^2 dV \sim G(l_c H_0/H_l^2)^2 H_l l_c^2$ with the work done by the pressure $pH_0 l_c^2$ yields

$$\eta \sim \frac{p}{G} \frac{H_l^3}{h_0 l_c^2}. \tag{162}$$

Since $l_c \sim \sqrt{h_0 R}$, (153), (155), and (162) yield

$$\eta \sim \frac{\mu V}{G} \frac{H_l^3}{h_0^{7/2} R^{1/2}}, \quad L_{\zeta \ll 1} \sim \frac{\mu^2 V^2}{G} \frac{H_l^3 R}{h_0^4}. \tag{163}$$

(e) For a thin poroelastic layer (Sec. VII), $l_c \sim \sqrt{h_0 R}$ and $\eta \sim [\mu(V-\omega R)/2G+\lambda](H_l R^{1/2}/h_0^{5/2})$, so that (155) yields

$$L_s \sim C(\gamma) \frac{\mu^2 V^2}{2G + \lambda} \frac{H_l R^2}{h_0^3}, \tag{164}$$

where γ is the ratio of the poroelastic time scale to the time scale of the motion.

(f) For a spherical shell slider (Sec. VIII) there are two cases: the thickness of the shell h_s is smaller than the gap thickness, i.e., $h_s \ll h_0$ and all the elastic energy is stored in stretching; or $h_s \gtrsim h_0$ and bending and stretching energies are of the same order of magnitude.[33] For a localized force, the deformation will be restricted to a region of area d^2. The stretching energy per unit area scales as $Gh_s H_0^2/R^2$, while the bending energy scales as $Gh_s^3 H_0^2/d^4$. The total elastic energy U of the deformation is then given by

$$U \approx \frac{Gh_s H_0^2 d^2}{R^2} + \frac{Gh_s^3 H_0^2}{d^2}, \tag{165}$$

which has a minimum at $d = \sqrt{h_s R}$. Comparing d with $l_c \sim \sqrt{h_0 R}$, we see that the hydrodynamic pressure is localized if $h_s > h_0$. For a localized force, $d = \sqrt{h_s R}$ while for a nonlocalized force, $d = R$. The elastic energy of a localized deformation, U_l, and a nonlocalized deformation, U_n, are given by

$$U_l = \frac{Gh_s^2 H_0^2}{R}, \quad U_n = Gh_s H_0^2. \tag{166}$$

The moment exerted by the hydrodynamic pressure on the spherical shell slider is

$$M \sim pl_c^3, \tag{167}$$

which is independent of h_0. The work done by the moment (167), which acts through an angle $\Delta\theta \sim H_0/d$, is

$$M\Delta\theta \sim pl_c^3 \frac{H_0}{d}. \tag{168}$$

Balancing the work done by the fluid (168) with the stored elastic energy (166) for both nonlocal and local deformations yields

$$\eta_n \sim \frac{\mu V R}{Gh_s h_0}, \quad \eta_l \sim \frac{\mu V R^{5/2}}{Gh_s^{5/2} h_0}, \tag{169}$$

so that (155) and (169) yield the lift force on the sphere for the two cases

$$L_l \sim \frac{\mu^2 V^2}{G} \frac{R^4}{h_s^{5/2} h_0^{3/2}} \quad \text{for } \frac{h_s}{h_0} \gg 1,$$
$$L_n \sim \frac{\mu^2 V^2}{G} \frac{R^{5/2}}{h_s h_0^{3/2}} \quad \text{for } \frac{h_s}{h_0} \lesssim 1. \tag{170}$$

(g) For the ball and socket configurations, roughly the three-dimensional analog of the journal bearing (Sec. IX), $l_c \sim R$ and $\eta \sim [\mu\omega R^2 H_l/(2G+\lambda)h_0^3]$ so that the horizontal force is given by (155):

$$L_s \sim \frac{\mu\omega^2 R^2}{2G + \lambda} \frac{H_l R^4}{h_0^5}. \tag{171}$$

XI. DISCUSSION

The various combinations of geometry and material properties in this paper yield some simple results of great generality: the elastohydrodynamic interaction between soft surfaces immersed in a viscous fluid leads generically to a coupling between tangential and normal forces regardless of specific material properties or geometrical configurations. The fluid pressure deforms soft solid, thereby giving rise to a normal force. For small surface deformations, η = surface displacement/characteristic gap thickness $\ll 1$, the dimensionless normal force is linear in η. Increasing η (i.e., softening the material) increases the asymmetry but decreases the magnitude of the pressure. The competition between symmetry breaking, which dominates for small η, and

decreasing pressure, which dominates for large η, produces a maximum in the lift force as a function of η, the material's softness.

Additional complications such as nonlinearities and anisotropy in both the fluid and the solid, streaming potentials and current generated stresses[40,41] would clearly change some of our conclusions. However, the robust nature of the coupling between the tangential and the normal forces illustrated in this paper should persist and suggest both experiments and design principles for soft lubrication.

ACKNOWLEDGMENTS

The authors thank Mederic Argentina for assistance in using the AUTO2000 software package, and both Howard Stone and Tim Pedley for their thoughtful comments. We acknowledge support via the Norwegian Research Council (J.M.S.), the U.S. Office of Naval Research Young Investigator Program (L.M.), and the U.S. National Institutes of Health (L.M.).

APPENDIX: THE ELASTOHYDRODYNAMIC RECIPROCAL THEOREM

Jeffrey and Onishi[42] calculated the flow around a cylinder near a wall in a viscous fluid and found that translation produces no torque on the cylinder. Similarly, a rotating cylinder experiences no net force. We now consider how elastohydrodynamics will alter this force balance. First, we consider the torque on a translating cylinder,

$$\Gamma = \int R\mathbf{n} \times \boldsymbol{\sigma}_f \cdot \mathbf{n}\, dx, \tag{A1}$$

where $\mathbf{n}=(x/R,-1)$. Based on the scalings used in Sec. II, we write the dimensionless torque as

$$\Gamma = \frac{\sqrt{2}\mu V R^{1/2}}{h_0^{1/2}}\Gamma', \tag{A2}$$

so that the dimensionless version of (A1) is

$$\Gamma = \frac{1}{\varepsilon}\int \mathbf{n} \times \boldsymbol{\sigma}_f \cdot \mathbf{n}\, dx, \tag{A3}$$

where

$$\mathbf{n} = (2\varepsilon x, -1), \tag{A4}$$

and we have dropped the prime. Equation (A3) is evaluated using (8) yielding

$$\Gamma = \int \partial_z v_x|_{z=1+x^2} dx. \tag{A5}$$

We find $\partial_z v_x|_{z=1+x^2}$ by solving (7) with $\omega'=0$, so that

$$\Gamma = \int \left(\frac{1}{h} + \frac{h\partial_x p}{2}\right) dx, \tag{A6}$$

where positive Γ corresponds to a torque pointing out of the page in Fig. 1. We drop the prime and solve (7) to find

$$\Gamma = \int \partial_z v_x|_{z=h} dx = \int \left(\frac{1}{h} + \frac{h\partial_x p}{2}\right) dx. \tag{A7}$$

To calculate the torque for small deflections we need to include terms of order η^2, so that

$$p = p^{(0)} + \eta p^{(1)} + \eta^2 p^{(2)} + O(\eta^3). \tag{A8}$$

For $p^{(2)}$ (9), (10), and (25) yield a system:

$$\begin{aligned} \eta^2{:}0 &= \partial_x[6p^{(1)} + 3(1+x^2)^2\partial_x(p^{(0)}p^{(1)}) + (1+x^2)\partial_x(p^{(0)})^3 \\ &\quad + (1+x^2)^3\partial_x p^{(2)}], \\ 0 &= p^{(2)}(-\infty) = p^{(2)}(\infty). \end{aligned} \tag{A9}$$

The order η^2 pressure is found using MATHEMATICA5.0 (Ref. 43) to be

$$p^{(2)} = -\frac{87\,465x + 38\,815x^3 + 121\,394x^5 + 95\,062x^7 + 39\,237x^9 + 6699x^{11}}{5600(1+x^2)^8}. \tag{A10}$$

Consequently,

$$\Gamma = \frac{21\pi}{128}\eta^2 + O(\eta^4), \tag{A11}$$

so that elastohydrodynamic effects cause a cylinder translating from left to right above a substrate to rotate clockwise. When $\eta=O(1)$, we evaluate (A7) numerically and show $\Gamma(\eta)$ in Fig. 21.

We now consider a stationary cylinder rotating clockwise. In this case the governing dimensionless lubrication equations are

$$\begin{aligned} &\partial_z p = 0, \quad \partial_x p = \partial_{zz} v_x, \\ &\partial_x v_x + \partial_z v_z = 0, \\ &p(x \to -\infty, z) = 0, \quad p(x \to \infty, z) = 0, \\ &v_x(x, -\eta H) = 0, \quad v_x(x, 1+x^2) = -1, \\ &v_z(x, -\eta H) = 0, \quad v_z(x, 1+x^2) = -2x, \end{aligned} \tag{A12}$$

where we have used the scaling of Sec. II but with $(V - \omega R) \to \omega R$. We solve (A12) and find the familiar Reynolds

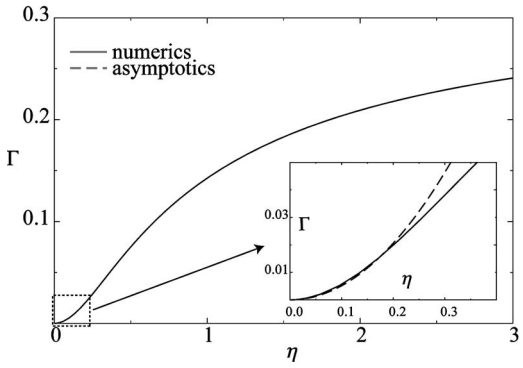

FIG. 21. Dimensionless torque Γ due to translation above a thin soft elastic layer. Surface deformation is needed to couple rotation to translation. For $\eta \ll 1$, $\Gamma = (21\pi/128)\eta$. A cylinder translating from left to right above a deformable substrate rotates clockwise.

equation, $0 = \partial_x(6h + h^3\partial_x p)$, $p(\pm\infty) = 0$, as well as the shear at the cylinder surface

$$\partial_z v_x|_{z=1+x^2} = -\frac{1}{h} + \frac{h\partial_x p}{2}. \tag{A13}$$

The Reynolds equation for the pressure is exactly the same as for the translating cylinder and produces an identical pressure field. The horizontal force on the cylinder is

$$F_x = \int \mathbf{e}_x \cdot \boldsymbol{\sigma}_f \cdot \mathbf{n} dx, \tag{A14}$$

where $\mathbf{e}_x = (1,0)$. Based on the scalings in Sec. II, we write the dimensional horizontal force as

$$F_x = \frac{\sqrt{2}\mu\omega R^{3/2}}{h_0^{1/2}} F_x'. \tag{A15}$$

After dropping primes (8), (A4), (A13), and (A14) yield

$$\begin{aligned} F_x &= \frac{1}{\varepsilon}\int \mathbf{e}_x \cdot \boldsymbol{\sigma}_f \cdot \mathbf{n}\, dx \\ &= \int (-\partial_z u_x|_{z=1+x^2} - 2xp) dx \\ &= \int \left(\frac{1}{h} - \frac{h\partial_x p}{2} - 2xp\right) dx. \end{aligned} \tag{A16}$$

Using Eqs. (A7) and (A16), we find the difference between the horizontal force on a rotating cylinder and the torque on a sliding cylinder in dimensionless terms,

$$\Gamma - F_x = \int (h\partial_x p + 2xp) dx. \tag{A17}$$

Since $h = 1 + x^2 + \eta p$, we have $2x = \partial_x h - \eta\partial_x p$ and

$$\Gamma - F_x = \int (h\partial_x p + p\partial_x h - \eta p\partial_x p) dx = hp - \frac{\eta}{2} p^2|_{-\infty}^{\infty} = 0. \tag{A18}$$

The linearity of Stokes' equations for viscous flow equations implies that we may linearly relate the force $\mathbf{F}$ and couple $\boldsymbol{\Gamma}$ with the velocity $\mathbf{V}$ and rate of rotation $\boldsymbol{\omega}$ via a matrix of second rank tensors so that

$$\begin{pmatrix} \mathbf{F} \\ \boldsymbol{\Gamma} \end{pmatrix} = \begin{pmatrix} \mathbf{A} & \mathbf{B} \\ \mathbf{C} & \mathbf{D} \end{pmatrix} \begin{pmatrix} \mathbf{V} \\ \boldsymbol{\omega} \end{pmatrix}. \tag{A19}$$

The reciprocal theorem for viscous flow[44] states that $\mathbf{B} = \mathbf{C}^T$. Due to the nonlinear coupling between translational and rotational modes, *a priori* there is no reason to expect any elastohydrodynamic analog to the reciprocal theorem. Nevertheless, for pure translation and rotation (A18) shows us that we may write

$$F_x = B(\eta)\omega, \quad \Gamma = C(\eta)V, \tag{A20}$$

where, somewhat surprisingly,

$$B(\eta) = C(\eta), \tag{A21}$$

and a cylinder rotating clockwise will translate in the x direction.

[1] B. J. Hamrock and D. Dowson, *Ball Bearing Lubrication: The Elastohydrodynamics of Elliptical Contacts* (Wiley, New York, 1981).
[2] O. Reynolds, "On the theory of lubrication and its application to Mr. Beauchamp Tower's experiments, including an experimental determination of the viscosity of olive oil," Philos. Trans. R. Soc. London **177**, 157 (1886).
[3] H. D. Conway and H. C. Lee, "The analysis of the lubrication of a flexible journal bearing," ASME J. Lubr. Technol. **97**, 599 (1975).
[4] D. Dowson and G. R. Higginson, "A numerical solution to the elastohydrodynamic problem," J. Mech. Eng. Sci. **1**, 7 (1959).
[5] B. J. Hamrock, *Fundamentals of Fluid Film Lubrication* (McGraw-Hill, New York, 1994).
[6] J. O'Donoghue, D. K. Brighton, and C. J. K. Hooke, "The effect of elastic distortions on journal bearing performance," ASME J. Lubr. Technol. **89**, 409 (1967).
[7] A. J. Grodzinsky, H. Lipshitz, and M. J. Glimcher, "Electromechanical properties of articular cartilage during compression and stress relaxation," Nature (London) **275**, 448 (1978).
[8] V. C. Mow and X. E. Guo, "Mechano-electrochemical properties of articular cartilage: their inhomogeneities and anisotropies," Annu. Rev. Biomed. Eng. **4**, 175 (2002).
[9] V. C. Mow, M. H. Holmes, and W. M. Lai, "Fluid transport and mechanical properties of articular cartilage: a review," J. Biomech. **17**, 377 (1984).
[10] E. R. Damiano, B. R. Duling, K. Ley, and T. C. Skalak, "Axisymmetric pressure-driven flow of rigid pellets through a cylindrical tube lined with a deformable porous wall layer," J. Fluid Mech. **314**, 163 (1996).
[11] J. Feng and S. Weinbaum, "Lubrication theory in highly compressible porous media: The mechanics of skiing, from red cells to humans," J. Fluid Mech. **422**, 281 (2000).
[12] J. M. Fitz-Gerald, "Mechanics of red-cell motion through very narrow capillaries," Proc. R. Soc. London, Ser. B **174**, 193 (1969).
[13] M. J. Lighthill, "Pressure-forcing of tightly fitting pellets along fluid-filled elastic tubes," J. Fluid Mech. **34**, 113 (1968).
[14] T. W. Secomb, R. Hsu, and A. R. Pries, "A model for red blood cell motion in glycocalyx-lined capillaries," Am. J. Physiol. **274**, H1016 (1998).
[15] T. W. Secomb, R. Skalak, N. Özkaya, and J. F. Gross, "Flow of axisymmetric red blood cells in narrow capillaries," J. Fluid Mech. **163**, 405 (1986).
[16] H. Tözeren and R. Skalak, "The steady flow of closely fitting incompressible elastic spheres in a tube," J. Fluid Mech. **87**, 1 (1978).
[17] W. Wang and K. H. Parker, "The effect of deformable porous surface layers on the motion of a sphere in a narrow cylindrical tube," J. Fluid Mech. **283**, 287 (1995).
[18] S. Weinbaum, X. Zhang, Y. Han, H. Vink, and S. Cowin, "Mechanotransduction and flow across the endothelial glycocalyx," Proc. Natl. Acad. Sci. U.S.A. **100**, 7988 (2003).

[19]R. I. Tanner, "An alternative mechanism for the lubrication of synovial joints," Phys. Med. Biol. **11**, 119 (1966).
[20]A. Martin, J. Clain, A. Buguin, and F. Brochard-Wyart, "Wetting transitions at soft, sliding interfaces," Phys. Rev. E **65**, 031605 (2002).
[21]J. Klein, D. Perahia, and S. Warburg, "Forces between polymer-bearing surfaces undergoing shear," Nature (London) **352**, 143 (1991).
[22]K. Sekimoto and L. Leibler, "A mechanism for shear thickening of polymer-bearing surfaces: elasto-hydrodynamic coupling," Europhys. Lett. **23**, 113 (1993).
[23]M. Abkarian, C. Lartigue, and A. Viallat, "Tank treading and unbinding of deformable vesicles in shear flow: Determination of the lift force," Phys. Rev. Lett. **88**, 068103 (2002).
[24]J. Beaucourt, T. Biben, and C. Misbah, "Optimal lift force on vesicles near a compressible substrate," Europhys. Lett. **67**, 676 (2004).
[25]L. G. Leal, "Particle motions in a viscous fluid," Annu. Rev. Fluid Mech. **12**, 435 (1980).
[26]F. Takemura, S. Takagi, J. Magnaudet, and Y. Matsumoto, "Drag and lift forces on a bubble rising near a vertical wall in a viscous fluid," J. Fluid Mech. **461**, 277 (2002).
[27]M. A. Biot, "General theory of three-dimensional consolidation," J. Appl. Phys. **12**, 155 (1941).
[28]L. G. Leal, *Laminar Flow and Convective Transport Processes: Scaling Principles and Asymptotic Analysis* (Butterworth-Heineman, Newton, MA, 1992).
[29]K. L. Johnson, *Contact Mechanics* (Cambridge University Press, Cambridge, UK, 1985).
[30]J. M. Skotheim and L. Mahadevan, "Soft lubrication," Phys. Rev. Lett. **92**, 245509 (2004).
[31]E. J. Doedel, R. C. Paffenroth, A. R. Champneys, T. F. Fairfrieve, Y. A. Kuznetsov, B. E. Oldeman, B. Sandstede, and X. Wang, AUTO2000: Continuation and Bifurcation Software for Ordinary Differential Equations, 2004.
[32]R. H. Davis, J.-M. Serayssol, and E. J. Hinch, "The elastohydrodynamic collision of two spheres," J. Fluid Mech. **163**, 479 (1986).
[33]L. D. Landau and E. M. Lifshitz, *Theory of Elasticity* (Pergamon, Oxford, UK, 1970).
[34]G. M. L. Gladwell, *Contact Problems in the Classical Theory of Elasticity* (Sijthoff and Noordhoff, Alphen aan den Rijn, The Netherlands, 1980).
[35]G. Cederbaum, L. P. Li, and K. Schulgasser, *Poroelastic Structures* (Elsevier, Oxford, UK, 2000).
[36]H. F. Wang, *Theory of Linear Poroelasticity with Applications to Geomechanics and Hydrogeology* (Princeton University Press, Princeton, NJ, 2000).
[37]J. M. Skotheim and L. Mahadevan, "Dynamics of poroelastic filaments," Proc. R. Soc. London, Ser. A **460**, 1995 (2004).
[38]S. I. Barry and M. Holmes, "Asymptotic behaviors of thin poroelastic layers," IMA J. Appl. Math. **66**, 175 (2001).
[39]A. E. H. Love, *A Treatise on the Mathematical Theory of Elasticity*, 4th ed. (Dover, New York, 1944).
[40]E. H. Frank and A. J. Grodzinsky, "Cartilage electromechanics. I. Electrokinetic transduction and the effects of electrolyte pH and ionic strength," J. Biomech. **20**, 615 (1987).
[41]E. H. Frank and A. J. Grodzinsky, "Cartilage electromechanics. II. A continuum model of cartilage electrokinetics and correlation with experiments," J. Biomech. **20**, 629 (1987).
[42]D. J. Jeffrey and Y. Onishi, "The slow motion of a cylinder next to a plane wall," Q. J. Mech. Appl. Math. **34**, 129 (1981).
[43]Wolfram Research, Inc., MATHEMATICA, Version 5.0, Champaign, IL, 2003.
[44]J. Happel and H. Brenner, *Low Reynolds Number Hydrodynamics* (Kluwer Boston, Hingham MA, 1983).